8-11-2020

Experimental And Theoretical Thermodynamic Studies Of Charging And Adsorption At The Solid-Aqueous Interface Of Aluminum-Bearing Ferrihydrites And Rutile

Faisal Torbu Adams

doi: https://doi.org/10.57709/18722340

EXPERIMENTAL AND THEORETICAL THERMODYNAMIC STUDIES OF CHARGING AND ADSORPTION AT THE SOLID-AQUEOUS INTERFACE OF ALUMINUM-BEARING FERRIHYDRITES AND RUTILE

by

FAISAL TORBU ADAMS

Under the Direction of Nadine Kabengi, PhD

ABSTRACT

In this thesis, three techniques are integrated to investigate how best to capture and parameterize complexity in interfacial reactions at mineral-aqueous interfaces. The first chapter employs a novel approach that leans on spectroscopic and computational data to build a Surface Complexation Model for aluminum-doped ferrihydrites. The model places Al on the surface in Fe1 sites and was found to fit empirical zeta potential measurements reasonably well. In chapter two, Flow Adsorption Microcalorimetry and Density Functional Theory calculations were each used to derive the enthalpies of phosphate, oxalate, and chromate sorption on the (110) face of rutile. The difficulty in determining the masses adsorbed in the experiment, and the complexity of electron interactions in our computational calculations, did not allow for a reconciliation of adsorption enthalpies. Although we successfully captured the complexity associated with substitution, we were unable to rationalize differences in deriving thermodynamics parameters.

INDEX WORDS: Flow calorimetry, MUSIC model, Computational modeling, enthalpies, SCM

EXPERIMENTAL AND THEORETICAL THERMODYNAMIC STUDIES OF CHARGING AND ADSORPTION AT THE SOLID-AQUEOUS INTERFACE OF ALUMINUM-BEARING FERRIHYDRITES AND RUTILE

by

FAISAL TORBU ADAMS

A Thesis Submitted in Partial Fulfillment of the Requirements for the Degree of

Master of Science

in the College of Arts and Sciences

Georgia State University

2020

EXPERIMENTAL AND THEORETICAL THERMODYNAMIC STUDIES OF CHARGING AND ADSORPTION AT THE SOLID-AQUEOUS INTERFACE OF ALUMINUM-BEARING FERRIHYDRITES AND RUTILE

by

FAISAL TORBU ADAMS

Committee Chair: Nadine Kabengi

Committee: Michael Machesky

Daniel Deocampo

Moira Ridley

Electronic Version Approved:

Office of Graduate Services

College of Arts and Sciences

Georgia State University

August 2020

DEDICATION

To Fati Ali-Yallah

ACKNOWLEDGEMENTS

I would like to say thank you to my family, who have been patient with me through this time as I got this work out. My profound gratitude goes to my Uncle Ali and his family for giving me a home during this time. I would also like to extend my gratitude to my advisor, Dr. Nadine Kabengi, who has gone above and beyond in her role as my advisor, as well as all members of Kabengi Lab. To one of the smartest people I know, thank you, Dr. Michael Machesky, for teaching me the ropes of complexation modeling, and being available for any and all questions I had, no matter how trivial. Similarly, I would like to thank Dr. James Kubicki for his insights on computational modeling. My gratitude goes to the Department of Geosciences at Georgia State University for the opportunities and chances to make life-long connections. This work would not be complete without the help of my close friend and colleague, Sean Zigah. Thank you for keeping an eye on me, and I will miss our in-depth conversations into all things, academic and otherwise.

TABLE OF CONTENTS

LIST OF TABLES

LIST OF FIGURES

LIST OF ABBREVIATIONS

FAMC – Flow Adsorption Micro-calorimetry

FMC – Flow Micro-calorimetry

SCM – Surface Complexation Model

MUSIC – MultiSite Ion Complexation

Fh – Ferrihydrite

Al-Fh – Aluminum doped Ferrihydrite

DFT – Density Functional Theory

MD – Molecular Dynamics

ZP – Zeta Potential

1 INTRODUCTION

Chemical reactions at mineral-water interfaces are of great interest to geochemists and colloidal scientists as they are fundamental to the retention and distribution of nutrients and contaminants in terrestrial and aqueous environments. For decades, researchers have employed various approaches and techniques (Parfitt and Smart 1978, Lasaga and Gibbs 1988, Wang et al. 2014, Lee et al. 2020) to understand and probe these surface interactions, e.g., adsorption, desorption, ion exchange, protonation, and deprotonation. Whereas some researchers utilize experimental techniques, such as calorimetry (Kabengi et al. 2006, Wu et al. 2015, Namayandeh and Kabengi 2019) and infrared spectroscopy (Johnston and Chrysochoou 2012, Johnston and Chrysochoou 2016), others employ empirical and theoretical approaches such as surface complexation models (Ridley et al. 2015, Machesky et al. 2019) and computational calculations that utilize first principles of physics to simulate and understand interactions (Pinney et al. 2009, Kubicki et al. 2012). These investigations have, alone and in tandem, led to a great deal of molecular-level understanding of interfacial reactions, mineral surfaces, and the interactions of the species in solution. Yet, it has become increasingly evident that a comprehensive and predictive understanding of interfacial reactions requires a holistic approach, which adequately represents realistic conditions by factoring in defects and impurities, and integrates various scales of data by tying experimental data with theoretical modeling. This thesis aims to help achieve the goal of merging both theory and practice in two systems - charging reactions of aluminum-doped ferrihydrite, and the adsorption of oxyanions on the rutile (110) face. The first seeks to incorporate increased complexity in attempts to model realistic surfaces, and the second reverts back to the utilization of a more straightforward system with the goal of examining the methodologies used.

1.1 Investigative thermodynamic techniques under study

In this thesis, three major techniques are explored and used in various degrees of entanglement. We first employ a surface complexation model (SCM) for its ease of use and versatility and apply it to an aluminum-doped iron (oxyhdr)oxide. In the latter section, an electrochemical technique, flow microcalorimetry, and computational calculations, Density Functional Theory (DFT), are benchmarked against each other to break down the complexity at play between their two scales. These two techniques are applied to the rutile (110) face, a well described and understood titanium oxide mineral surface (Diebold 2003, Bourikas et al. 2014).

1.1.1 Surface Complexation Modeling

Surface Complexation Models (SCMs) utilize a combination of surface chemical equilibrium equations with an interpretation of the electric double layer of the surface (Figure 1.1) to describe interactions between surface sites and aqueous species.

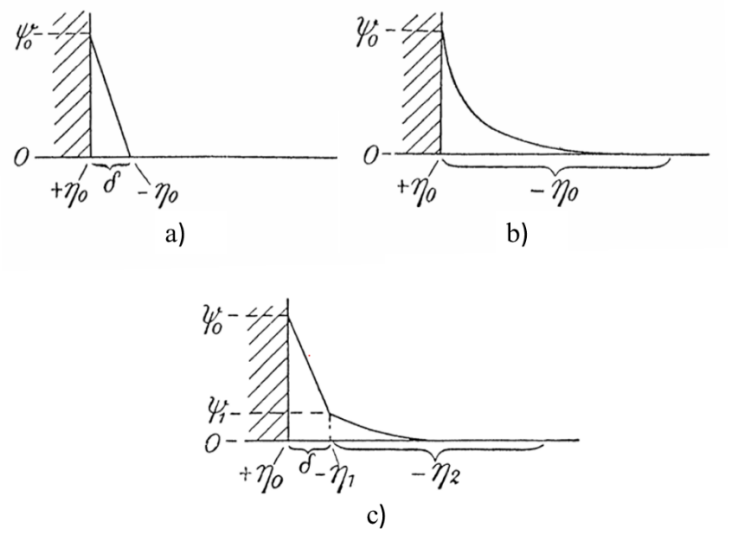

Figure 1.1. The (a) Helmholtz, (b) Gouy and Chapman, and (c) Stern models of the Electric Double Layer at solid-aqueous interfaces (Hiemstra and van Riemsdijk 2002.

There are several SCMs in use including but not limited to: the Constant Capacitance model (Sposito 1984), the Diffuse Double Layer model (Dzombak and Morel 1990), the Basic Stern model (Machesky et al. 1998) and the Triple Layer model (Davis and Leckie 1978). These SCMs aim to describe adsorption phenomena by iteratively solving chemical reaction equations and electrostatic interactions to equilibrium. The different SCMs vary in their methods of defining interfacial chemical reactions and the contribution of the aforementioned electrical components. Of these SCMs, the MultiSite Complexation (MUSIC) model has been the most successful at estimating the proton affinity of Fe and Al oxides (Hiemstra et al. 1989, Hiemstra et al. 1999). An extension of this model, the Charge Distribution MultiSite Complexation (CD-MUSIC) model was introduced to account for the spatial distribution of adsorbed charged ions within the interfacial region, a principle not applied previously in other conventional SCM models (Hiemstra and Van Riemsdijk 1996, Hiemstra and Van Riemsdijk 2000). The CD-MUSIC model acknowledges that surface complexes do not exist as point charges and accounts for the effect of their binding geometry (Hiemstra and Van Riemsdijk 1996).

1.1.2 Flow Adsorption Microcalorimetry

Flow microcalorimeters (FMC) measure minute heat changes associated with reactions within solutions. Early work involving FMCs aimed to determine thermodynamic and kinetic parameters, such as heat capacities (Picker et al. 1971, Desnoyers et al. 1976), enthalpies of dilution (Fortier et al. 1973), and reaction rates (Johnson and Biltonen 1975) of solutions and solvents, both organic and inorganic. With time, FMCs were used to study sorption phenomena between solutions and solids (Joslin and Fowkes 1985), and in this study, this approach that involves a stationary solid surface is termed Flow Adsorption Microcalorimetry (FAMC). Some more recent works involving FAMC, namely from our group have studied a plethora of surfaces

and solutions aimed at studying the implications of their interfacial interactions (Appel et al. 2013, Hawkins et al. 2017, Situm et al. 2017, Allen et al. 2019, Laudadio et al. 2019, Namayandeh and Kabengi 2019, Knight et al. 2020). FAMC provides the benefits of not being restricted by optic interferences, unlike classic spectroscopic techniques, and the ability to vary solution conditions without terminating the current experimental run. This approach has been successfully used to determine the energetics of ion exchange, and these values have served as a probe for determining the charge and structural characteristics of surfaces. FAMC has also been used to measure the energetics and reversibility of oxyanions that attach more strongly, offering an insight into the types of complexes forming. For example, Laudadio et al. (2019) complemented their spectroscopic analyses of phosphate adsorption on nanoparticles of $LiCoO_2$ with FAMC measurements, and these contributed to proposing a two-step mechanism for bidentate inner-sphere binding of phosphate.

1.1.3 Density Functional Theory Calculations

Computational studies have, for decades, been used to describe interatomic, intramolecular, and intermolecular interactions, with many investigations focusing on mineral-aqueous interfaces (Car and Parrinello 1985, Ogasawara et al. 2002, Bhandari et al. 2010, Ajayi and Kubicki 2020). Various computational techniques have been used to this effect - classical molecular mechanics (CMM) simulations and Density Functional Theory (DFT) calculations are two examples. While CMM simulations can assess nanometer-sized systems containing millions of atoms on the millisecond timescale, the accuracy of the method is still limited by the accuracy of the parameters employed. These parameters, commonly referred to as a force field, seek to dictate atomic interactions during simulations and are usually specialized towards specific moieties such as water, organics, clay minerals, etc. (Gaigeot and Sulpizi 2016, Kubicki and Ohno 2020).

These constraints also prevent the breaking and forming of bonds during CMM simulations, so chemical reactions, which are an integral aspect of interfacial processes, cannot be simulated.

DFT uses quantum mechanical principles to calculate electronic (and nuclear) structures, successfully circumventing the need for parameterization that plagues the classical approach. It can provide information on and predict thermodynamic properties, chemical bonds, and, therefore, spectroscopic properties as well (Car and Parrinello 1985). Although DFT does not require fitting parameters like the classical approach, possible structures can be constrained using experimental and spectroscopic data (Kubicki and Ohno 2020). DFT has been successfully used to study the adsorption of pollutants such as O_3, SO_2 (Rastegar et al. 2014), and acrolein (Rastegar et al. 2013) as a pathway to developing gas sensors. It has also been used to study magnetism (Assadi and Hanaor 2013), and to infer physical properties such as hardness (Music et al. 2016).

1.2 Mineral Surfaces

Two synthetic minerals are investigated in this thesis, chosen for properties unique to each. The first mineral explored is Aluminum-doped Ferrihydrite (Al-Fh) studied for the uncertainty surrounding its structure and the complexity of its surface. Both zeta potential measurements and an SCM of the surface are utilized here. The next section focuses on the rutile (110) face, which is very well researched and understood. The techniques used are FAMC and DFT, and their thermodynamic results compared and contrasted.

1.2.1 Ferrihydrite and Al-Ferrihydrite

Ferrihydrite (Fh) is an environmentally common iron oxyhydroxide that has relatively large specific surface areas reported between ~230 m^2/g and ~1250 m^2/g (Villalobos and Antelo 2011), which afford it high surface reactivity and sorptive capacity (Cornell and Schwertmann 2003,

Postma et al. 2007, Hiemstra and Van Riemsdijk 2009, Kabengi et al. 2017). Fh plays a vital role in the sequestration and cycling of environmentally relevant contaminants and nutrients and has been investigated for various applications, most notably water treatment (Ruby et al. 2016, Morone et al. 2019, Yang et al. 2020).

Over the years, various models (Figure 1.2) have been proposed for the structure of Fh (Drits et al. 1993, Manceau and Gates 1997, Michel et al. 2007). Drits et al. (1993) proposed a model comprised of three phases: defect-free, defect rich, and hematite-like. The model, however, was contradicted by Michel et al. (2007), who put forth a defect-free structure for Fh that contains both tetrahedrally- and octahedrally- coordinated Fe. Recently, a search involving over 5000 unique configurations of the Fh structure using ab initio DFT calculations determined that although several possible structures including that proposed by Michel et al. (2007) had viable low enthalpy structures, only the 2007 Michel model resulted in calculated Pair Distribution Function and X-ray Diffraction patterns consistent with their experimentally measured counterparts (Sassi and Rosso 2019). The presence of abundant elements in nature, like Silicon (Si) and Aluminum (Al), which can substitute into the Fh structure, further complicate the attempt to understand its structure. Consequently, there have been several investigations into the effect of Al substitution on crystallinity and reactivity of Fh (Hansel et al. 2011, Adra et al. 2013, Massey et al. 2014, Johnston and Chrysochoou 2016, Namayandeh and Kabengi 2019). The location of Al, however, within the structure of Fh and on the aluminum substituted Fh (Al-Fh) surface is not entirely understood (Cismasu et al. 2012, Manceau and Gates 2013).

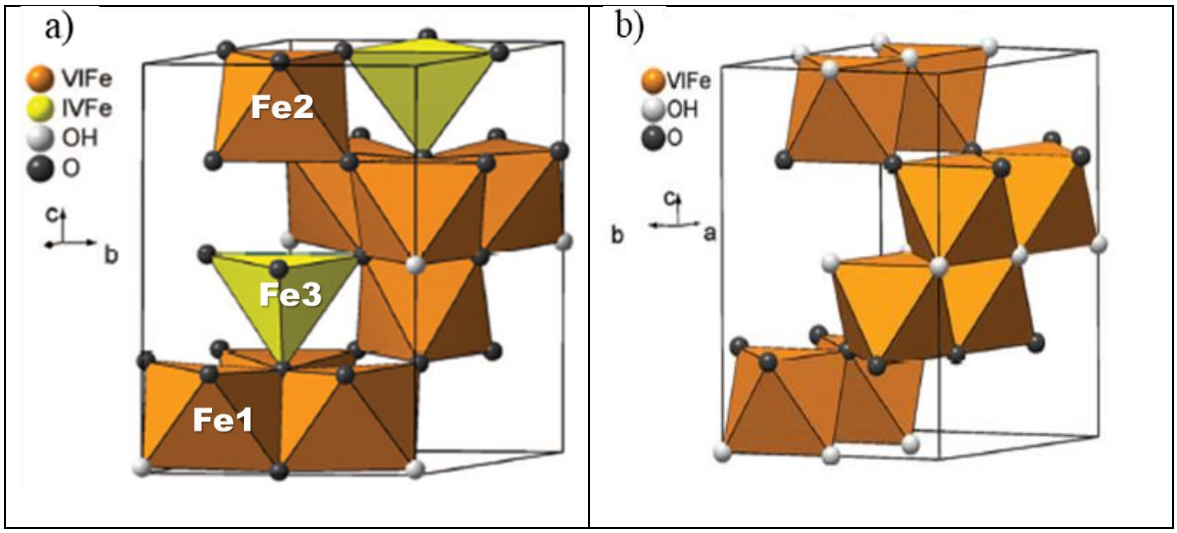

Figure 1.2 The (a) Michel et al. (2007) Keggin model showing the Fe1 and Fe2 octahedra, and the Fe3 tetrahedra. (b) The Drits f-phase model for Ferrihydrite (Manceau and Gates, 2013).

There has been at least one attempt by Manceau and Gates (2013) to describe the bulk structure of Al-Fh. This model did not define a surface structure. Neither did it state whether the surface would be representative of the core, or have a completely different makeup (Manceau and Gates 2013).

1.2.2 Rutile

Rutile is one of the more common polymorphs of titanium dioxide and has a wide range of applications – it is used as a photocatalyst in solar cells and as the white pigment of some paints (Diebold 2003). Its bulk structure consists of hexa-coordinated Ti atoms forming distorted TiO_6 octahedra in a tetragonal structure (Bourikas et al. 2014). Of interest to geochemists, however, are the interfacial reactions at the rutile surface, especially those involving the (110) crystal face that has been widely studied. There are several reasons for this focus – the (110) crystal face is the dominant and most stable crystal face. Additionally, synthetic rutile crystals with the (110) face predominant are relatively easy to produce and readily available. The termination of the rutile crystal lattice at this face results in undercoordinated Ti and O atoms of 5 and 2 coordination,

respectively. This deficiency results in the development of surface charge that greatly influences interfacial reactions and is influenced by solution pH. The pH_{znpc} charge, the pH at which the net charge on the rutile surface equals zero, has been reported to be 5.4 at 25°C (Ridley et al. 2002). There is little ambiguity concerning the rutile-aqueous interface, especially at the (110) face since extensive investigations have been carried out on its near-surface properties (Bourikas et al. 2014). These include the adsorption of water at the surface (Předota et al. (2004), as well as the interaction of surface sites and ions (Hiemstra et al. 1996, Zhang et al. 2004). For all intents and purposes, rutile and, in particular, its (110) face have become the archetypical surface for studies of mineral-water interfaces.

1.3 Overview

This thesis aims to reconcile theoretical, empirical and experimental approaches to understanding mineral-surface interactions while traversing various levels of complexity. This goal is achieved by using experimental data to complement a modeling approach in one case. The other scenario seeks to investigate the mechanisms linking two different methods, one computational and one experimental in obtaining thermodynamics parameters. A common theme of this work is "complexity". On one end, we seek to build complexity to better model the "real world" implications of one surface. On the other end, we aim to deconvolve some "real world" data to understand its underlying molecular-scale mechanisms better while allowing a real-time benchmarking of the techniques used.

In Chapter 2, we develop a novel SCM approach that leans on a host of experimental and computational data to account for defects and substitution in minerals. This approach is applied to Al-doped Ferrihydrites, and the SCM is used to fit experimental zeta potential data on that solid.

Chapter 3 explores measured and calculated energetics involved in the sorption of phosphate, chromate, and oxalate on rutile at pH 3.0. Both techniques, FAMC and DFT, are benchmarked against each other on the rutile (110) face, and this constraint to one surface eliminates much of the complexity and aids in investigating the discrepancies in the adsorption enthalpies obtained.

REFERENCES

Adra, A., G. Morin, G. Ona-Nguema, N. Menguy, F. Maillot, C. Casiot, O. Bruneel, S. Lebrun, F. Juillot & J. Brest (2013) Arsenic Scavenging by Aluminum-Substituted Ferrihydrites in a Circumneutral pH River Impacted by Acid Mine Drainage. *Environmental Science & Technology,* 47**,** 12784-12792.

Ajayi, O. A. & J. D. Kubicki (2020) Interfacial energies of supercritical CO2 and water with 2:1 layered silicate surfaces: A density functional theory study. *Applied Geochemistry,* 114**,** 104514.

Allen, N., C. Dai, Y. Hu, J. D. Kubicki & N. Kabengi (2019) Adsorption Study of Al3+, Cr3+, and Mn2+ onto Quartz and Corundum using Flow Microcalorimetry, Quartz Crystal Microbalance, and Density Functional Theory. *ACS Earth and Space Chemistry,* 3**,** 432-441.

Appel, C., D. Rhue, N. Kabengi & W. Harris (2013) Calorimetric investigation of the nature of sulfate and phosphate sorption on amorphous aluminum hydroxide. *Soil Science,* 178**,** 180-188.

Assadi, M. H. N. & D. A. H. Hanaor (2013) Theoretical study on copper's energetics and magnetism in TiO2 polymorphs. *Journal of Applied Physics,* 113**,** 233913.

Bhandari, N., D. B. Hausner, J. D. Kubicki & D. R. Strongin (2010) Photodissolution of Ferrihydrite in the Presence of Oxalic Acid: An In Situ ATR-FTIR/DFT Study. *Langmuir,* 26**,** 16246-16253.

Bourikas, K., C. Kordulis & A. Lycourghiotis (2014) Titanium Dioxide (Anatase and Rutile): Surface Chemistry, Liquid–Solid Interface Chemistry, and Scientific Synthesis of Supported Catalysts. *Chemical Reviews,* 114**,** 9754-9823.

Car, R. & M. Parrinello (1985) Unified Approach for Molecular Dynamics and Density-Functional Theory. *Physical Review Letters,* 55**,** 2471-2474.

Cismasu, A. C., F. M. Michel, J. F. Stebbins, C. Levard & G. E. Brown (2012) Properties of impurity-bearing ferrihydrite I. Effects of Al content and precipitation rate on the structure of 2-line ferrihydrite. *Geochimica et Cosmochimica Acta,* 92**,** 275-291.

Cornell, R. M. & U. Schwertmann. 2003. *The iron oxides: structure, properties, reactions, occurrences and uses*. John Wiley & Sons.

Desnoyers, J. E., C. de Visser, G. Perron & P. Picker (1976) Reexamination of the heat capacities obtained by flow microcalorimetry. Recommendation for the use of a chemical standard. *Journal of Solution Chemistry,* 5**,** 605-616.

Diebold, U. (2003) The surface science of titanium dioxide. *Surface Science Reports,* 48**,** 53-229.

Drits, V. A., B. A. Sakharov, A. L. Salyn & A. Manceau (1993) Structural Model for Ferrihydrite. *Clay Minerals,* 28**,** 185-207.

Fortier, J. L., P. A. Leduc, P. Picker & J. E. Desnoyers (1973) Enthalpies of dilution of electrolyte solutions by flow microcalorimetry. *Journal of Solution Chemistry,* 2**,** 467-475.

Gaigeot, M.-P. & M. Sulpizi (2016) Mineral/Water Interaction. *Molecular Modeling of Geochemical Reactions***,** 271-309.

Hansel, C. M., D. R. Learman, C. J. Lentini & E. B. Ekstrom (2011) Effect of adsorbed and substituted Al on Fe(II)-induced mineralization pathways of ferrihydrite. *Geochimica et Cosmochimica Acta,* 75**,** 4653-4666.

Hawkins, T., N. Allen, M. L. Machesky, D. J. Wesolowski & N. Kabengi (2017) Ion Exchange Thermodynamics at the Rutile–Water Interface: Flow Microcalorimetric Measurements and Surface Complexation Modeling of Na–K–Rb–Cl–NO3 Adsorption. *Langmuir,* 33**,** 4934-4941.

Hiemstra, T. & W. H. Van Riemsdijk (2009) A surface structural model for ferrihydrite I: Sites related to primary charge, molar mass, and mass density. *Geochimica et Cosmochimica Acta,* 73**,** 4423-4436.

Hiemstra, T., P. Venema & W. H. V. Riemsdijk (1996) Intrinsic Proton Affinity of Reactive Surface Groups of Metal (Hydr)oxides: The Bond Valence Principle. *Journal of Colloid and Interface Science,* 184**,** 680-692.

Johnson, R. E. & R. L. Biltonen (1975) Determination of reaction rate parameters by flow microcalorimetry. *Journal of the American Chemical Society,* 97**,** 2349-2355.

Johnston, C. P. & M. Chrysochoou (2012) Investigation of chromate coordination on ferrihydrite by in situ ATR-FTIR spectroscopy and theoretical frequency calculations. *Environ Sci Technol,* 46**,** 5851-8.

Johnston, C. P. & M. Chrysochoou (2016) Mechanisms of chromate, selenate, and sulfate adsorption on al-substituted ferrihydrite: implications for ferrihydrite surface structure and reactivity. *Environmental science & technology,* 50**,** 3589-3596.

Joslin, S. T. & F. M. Fowkes (1985) Surface acidity of ferric oxides studied by flow microcalorimetry. *Industrial & Engineering Chemistry Product Research and Development,* 24**,** 369-375.

Kabengi, N. J., M. Chrysochoou, N. Bompoti & J. D. Kubicki (2017) An integrated flow microcalorimetry, infrared spectroscopy and density functional theory approach to the study of chromate complexation on hematite and ferrihdyrite. *Chemical Geology,* 464**,** 23-33.

Kabengi, N. J., R. D. Rhue & S. H. Daroub (2006) Using Flow Calorimetry to Determine the Molar Heats of Cation and Anion Exchange and the Point of Zero Net Charge on Amorphous Aluminum Hydroxides. *Soil Science,* 171**,** 13-20.

Knight, A. W., P. Ilani-Kashkouli, J. A. Harvey, J. A. Greathouse, T. A. Ho, N. Kabengi & A. G. Ilgen (2020) Interfacial reactions of Cu(ii) adsorption and hydrolysis driven by nano-scale confinement. *Environmental Science: Nano,* 7**,** 68-80.

Kubicki, J. D., M. Aryanpour, L. Kabalan & Q. Zhu (2012) Quantum mechanical calculations on FeOH nanoparticles. *Geoderma,* 189-190**,** 236-242.

Kubicki, J. D. & T. Ohno (2020) Integrating Density Functional Theory Modeling with Experimental Data to Understand and Predict Sorption Reactions: Exchange of Salicylate for Phosphate on Goethite. *Soil Systems,* 4**,** 27.

Lasaga, A. C. & G. V. Gibbs (1988) Quantum mechanical potential surfaces and calculations on minerals and molecular clusters. *Physics and Chemistry of Minerals,* 16**,** 29-41.

Laudadio, E. D., P. Ilani-Kashkouli, C. M. Green, N. J. Kabengi & R. J. Hamers (2019) Interaction of Phosphate with Lithium Cobalt Oxide Nanoparticles: A Combined Spectroscopic and Calorimetric Study. *Langmuir,* 35**,** 16640-16649.

Lee, S. S., C. Park, N. C. Sturchio & P. Fenter (2020) Nonclassical Behavior in Competitive Ion Adsorption at a Charged Solid–Water Interface. *The Journal of Physical Chemistry Letters,* 11**,** 4029-4035.

Machesky, M. L., M. K. Ridley, D. Biriukov, O. Kroutil & M. Předota (2019) Oxalic Acid Adsorption on Rutile: Experiments and Surface Complexation Modeling to 150 °C. *Langmuir,* 35**,** 7631-7640.

Manceau, A. & W. P. Gates (1997) Surface structural model for ferrihydrite. *Clays and Clay Minerals,* 45**,** 448-460.

Manceau, A. & W. P. Gates (2013) Incorporation of Al in iron oxyhydroxides: implications for the structure of ferrihydrite. *Clay Minerals,* 48**,** 481-489.

Massey, M. S., J. S. Lezama-Pacheco, F. M. Michel & S. Fendorf (2014) Uranium incorporation into aluminum-substituted ferrihydrite during iron(ii)-induced transformation. *Environmental Science: Processes & Impacts,* 16**,** 2137-2144.

Michel, F. M., L. Ehm, S. M. Antao, P. L. Lee, P. J. Chupas, G. Liu, D. R. Strongin, M. A. A. Schoonen, B. L. Phillips & J. B. Parise (2007) The Structure of Ferrihydrite, a Nanocrystalline Material. *Science,* 316**,** 1726.

Morone, A., P. Mulay & S. P. Kamble. 2019. 8 - Removal of pharmaceutical and personal care products from wastewater using advanced materials. In *Pharmaceuticals and Personal Care Products: Waste Management and Treatment Technology,* eds. M. N. V. Prasad, M. Vithanage & A. Kapley, 173-212. Butterworth-Heinemann.

Music, D., R. W. Geyer & J. M. Schneider (2016) Recent progress and new directions in density functional theory based design of hard coatings. *Surface and Coatings Technology,* 286**,** 178-190.

Namayandeh, A. & N. Kabengi (2019) Calorimetric study of the influence of aluminum substitution in ferrihydrite on sulfate adsorption and reversibility. *Journal of Colloid and Interface Science,* 540**,** 20-29.

Ogasawara, H., B. Brena, D. Nordlund, M. Nyberg, A. Pelmenschikov, L. G. M. Pettersson & A. Nilsson (2002) Structure and Bonding of Water on Pt(111). *Physical Review Letters,* 89**,** 276102.

Parfitt, R. L. & R. S. C. Smart (1978) The Mechanism of Sulfate Adsorption on Iron Oxides *Soil Science Society of America Journal,* 42**,** 48-50.

Picker, P., P.-A. Leduc, P. R. Philip & J. E. Desnoyers (1971) Heat capacity of solutions by flow microcalorimetry. *The Journal of Chemical Thermodynamics,* 3**,** 631-642.

Pinney, N., J. D. Kubicki, D. S. Middlemiss, C. P. Grey & D. Morgan (2009) Density Functional Theory Study of Ferrihydrite and Related Fe-Oxyhydroxides. *Chemistry of Materials,* 21**,** 5727-5742.

Postma, D., F. Larsen, N. T. Minh Hue, M. T. Duc, P. H. Viet, P. Q. Nhan & S. Jessen (2007) Arsenic in groundwater of the Red River floodplain, Vietnam: Controlling geochemical processes and reactive transport modeling. *Geochimica et Cosmochimica Acta,* 71**,** 5054-5071.

Předota, M., A. V. Bandura, P. T. Cummings, J. D. Kubicki, D. J. Wesolowski, A. A. Chialvo & M. L. Machesky (2004) Electric Double Layer at the Rutile (110) Surface. 1. Structure of Surfaces and Interfacial Water from Molecular Dynamics by Use of ab Initio Potentials. *The Journal of Physical Chemistry B,* 108**,** 12049-12060.

Rastegar, S. F., N. L. Hadipour & H. Soleymanabadi (2014) Theoretical investigation on the selective detection of SO2 molecule by AlN nanosheets. *Journal of Molecular Modeling,* 20**,** 2439.

Rastegar, S. F., N. L. Hadipour, M. B. Tabar & H. Soleymanabadi (2013) DFT studies of acrolein molecule adsorption on pristine and Al-doped graphenes. *Journal of molecular modeling,* 19**,** 3733-3740.

Ridley, M. K., M. L. Machesky & J. D. Kubicki (2015) Experimental Study of Strontium Adsorption on Anatase Nanoparticles as a Function of Size with a Density Functional Theory and CD Model Interpretation. *Langmuir,* 31**,** 703-713.

Ridley, M. K., M. L. Machesky, D. A. Palmer & D. J. Wesolowski (2002) Potentiometric studies of the rutile–water interface: hydrogen-electrode concentration-cell versus glass-electrode titrations. *Colloids and Surfaces A: Physicochemical and Engineering Aspects,* 204**,** 295-308.

Ruby, C., S. Naille, G. Ona-Nguema, G. Morin, M. Mallet, D. Guerbois, K. Barthélémy, M. Etique, A. Zegeye, Y. Zhang, H. Boumaïza, M. Al-Jaberi, A. Renard, V. Noël, P. Binda, K. Hanna, C. Despas, M. Abdelmoula, R. Kukkadapu, J. Sarrias, M. Albignac, P. Rocklin, F. Nauleau, N. Hyvrard & J.-M. Génin (2016) Use of Ferrihydrite-Coated Pozzolana and Biogenic Green Rust to Purify Waste Water Containing Phosphate and Nitrate. *Current Inorganic Chemistry,* 6**,** 100-118.

Sassi, M. & K. M. Rosso (2019) Roles of Hydration and Magnetism on the Structure of Ferrihydrite from First Principles. *ACS Earth and Space Chemistry,* 3**,** 70-78.

Situm, A., M. A. Rahman, N. Allen, N. Kabengi & H. A. Al-Abadleh (2017) ATR-FTIR and Flow Microcalorimetry Studies on the Initial Binding Kinetics of Arsenicals at the Organic-Hematite Interface. *J Phys Chem A,* 121**,** 5569-5579.

Villalobos, M. & J. Antelo (2011) A unified surface structural model for ferrihydrite: Proton charge, electrolyte binding, and arsenate adsorption. *Revista Internacional de Contaminación Ambiental,* 27**,** 139-151.

Wang, H.-W., M. J. DelloStritto, N. Kumar, A. I. Kolesnikov, P. R. C. Kent, J. D. Kubicki, D. J. Wesolowski & J. O. Sofo (2014) Vibrational Density of States of Strongly H-Bonded Interfacial Water: Insights from Inelastic Neutron Scattering and Theory. *The Journal of Physical Chemistry C,* 118**,** 10805-10813.

Wu, D., T. M. McDonald, Z. Quan, S. V. Ushakov, P. Zhang, J. R. Long & A. Navrotsky (2015) Thermodynamic complexity of carbon capture in alkylamine-functionalized metal–organic frameworks. *Journal of Materials Chemistry A,* 3**,** 4248-4254.

Yang, Y., J. Lohwacharin, S. Takizawa & L.-a. Hou (2020) Comparison between ferrihydrite adsorption and full-scale advanced drinking water treatment processes for controlling bacterial regrowth potential. *Chemosphere,* 241**,** 125001.

Zhang, Z., P. Fenter, L. Cheng, N. C. Sturchio, M. J. Bedzyk, M. Předota, A. Bandura, J. D. Kubicki, S. N. Lvov, P. T. Cummings, A. A. Chialvo, M. K. Ridley, P. Bénézeth, L. Anovitz, D. A. Palmer, M. L. Machesky & D. J. Wesolowski (2004) Ion Adsorption at the Rutile−Water Interface: Linking Molecular and Macroscopic Properties. *Langmuir,* 20**,** 4954-4969.

2 A NOVEL SURFACE COMPLEXATION MODELING APPROACH FOR SUBSTITUTION IN MINERALS – A CASE STUDY OF ALUMINUM FERRIHYDRITES.

2.1 Introduction

Surface Complexation Models (SCMs) have been successfully applied to describe and predict surface protonation and ion sorption at a host of interfaces, involving metal oxides (Waite et al. 1994, Hiemstra et al. 1999, Spathariotis and Kallianou 2007, Hawkins et al. 2017), clay surfaces (Payne et al. 2004) and under a range of temperatures going up to 250ºC (Machesky et al. 1998, Fedkin et al. 2003, Machesky et al. 2015). Although most SCMs could describe interfacial reactions fairly well (Goldberg 1992), the parameters used in these early models were not based on specific experimental data for the systems studied (Machesky et al. 2015). As such, one experimental data set could be modeled by several different yet plausible sets of parameter values. The advent of cutting-edge spectroscopic and computational modeling techniques, however, aided in selecting unique parameters by providing constraints based on accurate data, molecular-level of the surface and interface. The Charge Distribution (CD) extension to the Multisite Complexation (MUSIC) model developed by Hiemstra and Van Riemsdijk (1996) assigned charges to surface groups based on their structural coordination and was successfully used to model PO_4 sorption on goethite. Subsequently, the CD-MUSIC approach has been utilized in numerous ways, for example, by Rietra et al. (1999). They constrained the stochiometry in their model based on spectroscopically observed surface complexes for a host of oxyanions on goethite. Similarly, Zhang et al. (2004) utilized ab initio bond length and partial charges to determine the proton affinities for surface oxygens on rutile.

Still, and for the most part, the utilization of SCMs has remained limited to idealized surfaces and single-phase minerals, which are, however, not representative of environmentally prevalent and relevant surfaces. There have been some attempts to simulate substitution-doped metal oxides and more complex mineral assemblages typically found in natural environments. These approaches consisted of either combining the parameters of the end members or assigning uniform values for intrinsic affinity constants and site densities to the entire mineral surface. For instance, using a non-electrostatic SCM, Pagnanelli et al. (2006) modeled protonation and lead (Pb) sorption for a mixture of quartz, muscovite, clinochlore, goethite, and hematite by adding the proton binding values of all individual components. Similalry, Reich et al. (2010) modeled Pb sorption on mixtures of hydrous ferric oxide, quartz, and kaolinite using the diffuse Double Layer Model (DLM) (Dzombak and Morel 1990) and a component additivity approach, i.e., summing the parameters for the pure end members. On the other hand, Spathariotis and Kallianou (2007) used both the Constant Capacitance Model and the DLM to fit the adsorption of copper (Cu), zinc (Zn) and cadmium (Cd) on Al substituted (Al-Gh) goethite. The authors assigned a uniform site density and binding constant value to the whole surface and compared the results from these two models. Although Ainsworth et al. (1989) assigned a singular site density to their mineral surface, they accounted for the individual binding constants of surface groups in modeling chromate adsorption on Al-Gh using the Triple Layer Model. However, none of these attempts is entirely realistic as the approaches do not account for the impact of the substitutions' location on the overall reactivity of the modified surfaces.

Ferrihydrite (Fh) is one such iron oxyhydroxide whose structure, after decades of deliberation (Drits et al. 1993, Manceau and Gates 1997, Gilbert et al. 2013), has been suggested to possess defects. The latest model, proposed by Michel et al. (2007) has been widely scrutinized

and seemingly corroborated by spectroscopic methods that showed isolated Keggin-like Fe clusters aggregating into Fh nanoparticles (Sadeghi et al. 2015) and computational models that calculated Pair Distribution Function and X-ray Diffraction patterns consistent with empirically-measured counterparts (Sassi and Rosso 2019). A surface depletion model for Fh developed by (Hiemstra 2013) provided insights into the structure of the Fh nanoparticle and informed a surface that catered to defects. This surface possessed 11 reactive sites consisting of singly-coordinated surface groups that belong to Fe1 octahedra and facilitate double corner complexes and bidentate edge complexes, and triply-coordinated Fe surface groups that contribute to protonation. Bompoti et al. (2017) fit numerous past titration datasets on Fh using the CD-MUSIC approach based on this 11 site surface model and simplified three (3) site variants of it to a high degree of certainty. Similarly, PO_4 and CO_3 sorption were successfully modeled using the same surface model and SCM method (Mendez and Hiemstra 2019, Mendez and Hiemstra 2020).

Fh is commonly found doped with impurities such as silicon, Si, (Carlson and Schwertmann 1981, Vempati and Loeppert 1989) and aluminum, Al, (Adra et al. 2013, Adra et al. 2016) .The surface of Al-doped Fh (Al-Fh) is not as well understood as its undoped analog. Some studies have investigated the effects of Al doping and potential substitution on the overall structure (Cismasu et al. 2013) and surface reactivity of Fh (Hansel et al. 2011, Adra et al. 2013, Massey et al. 2014, Johnston and Chrysochoou 2016, Namayandeh and Kabengi 2019). Manceau and Gates (2013) investigated the location of Al substitutions in both the Michel and Drits models. They concluded that due to Al-Al avoidance, a maximum of 20% substitution could occur in the Michel model. Previous empirical studies had placed the upper limit of Al substitution higher at ~25 to ~30% (Cismasu et al. 2012). The authors also concluded that the f-phase model of (Drits et al. 1993) provided a better fit with Al occupying positions in alternating octahedral sites. The f-phase

model is comprised of three phases: defect-free, defect rich, and hematite-like, all of which are octahedrally coordinated Fe.

In this study, we propose a novel SCM approach for determining the surface structure resulting from doping in metal oxides. Based on clues and findings from spectroscopic (Cismasu et al. 2012, Cismasu et al. 2013), thermodynamic (Namayandeh and Kabengi 2019) and modeling studies (Bazilevskaya et al. 2011, Pinney and Morgan 2013), we hypothesized that Al substituted for the octahedrally-coordinated surface Fe (Fe1) sites. This replacement results in singly coordinated AlOH surface groups whose affinity constants we inferred from the literature. The substituted mineral surface was modified from Hiemstra's surface depletion model for Fh (Hiemstra 2013). The new SCM was used to model charging of undoped Fh (0Al Fh), 12 mol% Al (12 Al-Fh), and 24% Al (24 Al-Fh) Al doped Fh samples. Finally, we discuss the merit of our approach as a platform for future efforts to model environmentally relevant and realistic surfaces.

2.2 Modeling and Experimental Methods

2.2.1 Model Description

The surface complexation model (SCM) developed has two new features – an approach to account for Al substitution within the Fh model and a mechanism for simulating zeta potential data.

Approach to Describe the Al-Fh Surface

To account for the presence of Al in Fh, we first opted to investigate the reactivity of the Al-Fh surface. According to Hiemstra (2013), 11 sites consisting of both singly and triply coordinated Fe on the (110) and (111) faces of Fh nanoparticles are the most reactive over the typical environmentally accessible pH range (pH 4 to 10). Therefore, these sites dictate Fh's surface reactivity and sorption properties (Bompoti et al. 2017, Mendez and Hiemstra 2020).

Spectroscopic (Cismasu et al. 2013, Johnston and Chrysochoou 2016) and thermodynamic (Namayandeh and Kabengi 2019) investigations have demonstrated that Al affects the charging and sorptive properties of Fh even when a separate aluminum phase is not detected. Furthermore, in the idealized Fh structure, the singly-coordinated sites make up ~29% of all Fh surface sites, a value close to the proposed upper limit of Al substitution in Fh (~25% to ~30%). (Cismasu et al. 2012, Manceau and Gates 2013) Additionally, all singly-coordinated reactive sites can be found only on Fe1 sites, which are predominant and make up ~72% of the Fh nanoparticle (Hiemstra 2013). We postulate, therefore, that Al is substituting for these singly coordinated reactive sites on the surface and, in essence, replacing the Fe1 sites. To account for the presence of Al on the surface, we began with the 11-site model for Fh (Hiemstra 2013, Bompoti et al. 2017) and introduced four additional sites having Al-based parameters (log K_{H+} and charge distribution) . The values of the parameters for the "Al-sites" were informed from previous SCMs of Al-oxides and Al-doped minerals (Ainsworth et al. 1989, Hiemstra et al. 1999, Spathariotis and Kallianou 2007).

Table 2.1. The surface site types and their designations, the coordination, face distribution, site densities, charge, and the corresponding log K value from (Hiemstra 2013).

Four sites have been added, and as such, the site designations here differ from the designations used by (Hiemstra 2013)

Designation	Face	Face Distribution	Type	**Ns(nm^{-2})** 0% Al-Fh	Charge	log K1	log K2
s1	(1-10)	37.5	FeOH*a*	1.90	-0.5		10.4
s2			FeOH*b*	7.40	-0.5		8
s3			Fe3O*a*	3.70	-0.5	10.4	
s4			Fe3O*b*	1.90	-0.5	5.5	
s5			Fe3O*c*	3.70	-0.25	3.3	
s6			AlOH*a*	-	-0.5		11
s7			AlOH*b*	-	-0.5		9
s8	(1-11)	37.5	FeOH*c*	1.60	-0.5		10.4
s9			FeOH*d*	6.50	-0.5		8
s10			Fe3O*d*	3.30	-0.5	10.4	
s11			Fe3O*e*	3.30	-0.25	3.3	
s12			AlOH*c*	-	-0.5		11
s13			AlOH*d*	-	-0.5		9
s14	(001)	12.5	Fe3O*f*	1.10	-0.5	5.5	
s15	(00-1)	12.5	Fe3O*g*	1.10	-0.5	7.5	

Past research by (Bompoti et al. 2017) has proven that varying specific crystal face contributions influences the point of zero charge (pH_{znpc}) simulated by a model. Similarly, previous SCM models (Ainsworth et al. 1989, Spathariotis and Kallianou 2007) and experiments (Adra et al. 2013, Adra et al. 2016) on Al doped Fe-oxides have shown that these samples tend to have a higher pH_{znpc} than their undoped counterparts. In that vein, the extent of Al substitution in our SCM was controlled by attenuating the contribution of all singly-coordinated Fe sites while introducing singly-coordinated Al sites to keep the overall mineral surface site density constant. The extent of Al intrusion in our model was constrained by our experimental samples, which had Al contents of 12% and 24%. We represented the presence of Al by determining the number of sites equivalent to 12% and 24% of all present Fh surface sites and assigned those numbers solely to the singly coordinated Fe positions. Based on these calculations, ~12% of all surface sites is

equivalent to ~42% of singly-coordinated sites, and 24% of all surface sites equals ~84% of singly-coordinated sites. We believe these assumptions and our hypothesis that Al is replacing the Fe1 sites in Fh provide a plausible description of the Al-Fh surface.

Zeta Potential Modeling

Modeling the charge characteristics of the Al-Fh surfaces was difficult because, to our knowledge, there are no complete surface charge titration data sets for Al-Fh in the literature and no SCMs that utilized our approach to account for substitution. Without these data, it was not possible to determine the values needed to constrain the equations involved or the parameters that needed to be taken into account. Therefore, previously published results of zeta potential as a function of pH obtained by our research group were utilized and simulated. Most existing SCMs (Davis and Leckie 1980, Ainsworth et al. 1989, Spathariotis and Kallianou 2007, Machesky et al. 2015, Machesky et al. 2019) describe sorption and surface charging as a function of pH. Still, few have sought to model zeta potential effects and describe electrolyte interactions (Hiemstra et al. 1999, Fedkin et al. 2003). The parameters and methods involved in our model are specific surface area, protonation constants (log K_{H+}), binding constants for background electrolyte ions, and an electrical double layer model (in this case, the Basic Stern model, which reduces parameterization). The MUSIC method was utilized (Hiemstra et al. 1989, Hiemstra et al. 2009, Hiemstra 2010) since it has been successfully used to describe protonation on Fe-oxides (Bompoti et al. 2017) and Al-oxides (Hiemstra et al. 1999, Corral Valero et al. 2019).

Protonation log K constant values for all reactive Fe surface groups were obtained from previous SCMs for Fh (Hiemstra 2013, Bompoti et al. 2017) . The protonation constants, K, for singly- and triply-coordinated surface oxygens respectively for Fe in Fh were not changed from previously published values in those papers.

A Stern Layer capacitance of 0.92 Fm^{-2}, as derived by Nefeli et al. (2017), was adequate for curve fitting in our model and, as such, was unchanged. The relationship between the surface charge (σ_0), Stern layer capacitance and plane potential, as determined by the Basic Stern (BS) model, is given by;

$$\sigma_0 = C_{Stern}\,(\psi_0 - \psi_1) \quad (1)$$

where C_{Stern} = the capacitance of the Stern Layer, ψ_0 = potential at the 0 or surface plane, and ψ_1 = potential at the 1 or Stern plane. Using established values for Fh with no Al substitution (Hiemstra 2013, Bompoti et al. 2017), the zeta potential was modeled with constrained parameters for protonation, electrolyte ions binding and the Stern layer capacitance. As such, the slipping plane distance (Ds) was used as the optimization parameter to obtain the best fit between model-generated charging curves and the experimental l data consistent with the basic Stern layer model. The Ds value is understood to represent the slipping plane distance from the head of the diffuse layer, at which the zeta potential is expressed. (Hiemstra et al. 1999, Fedkin et al. 2003, Pate and Safier 2016) The following equation from (Fedkin et al. 2003), valid for 1:1 electrolytes, was used:

$$\zeta = \left(\frac{4RT}{F}\right) \text{arctanh}\,[\tanh\left[\frac{F\psi_d}{4RT}\right] exp(-kD_s) \quad (2)$$

where ψ_d = potential at the head of the diffuse layer, k = the Debye-Huckel parameter, D_s= the slipping plane distance from the head of the diffuse layer, R = gas constant, T = absolute temperature, and F = Faraday constant. The Debye-Huckel parameter, k, is in turn determined from:

$$k = \sqrt{\frac{(2F^2 m_{tot} \times 1000)}{\epsilon\epsilon_0 RT}}$$

Where m_{tot} = the total concentration of ions, ϵ = relative permittivity of a medium, ϵ_0 = permittivity of a vacuum, R = gas constant, and T = absolute temperature. The mathematical

construct of the zeta potential model was developed from modified Mathematica notebooks for Fh (Bompoti et al. 2017) and run within Wolfram Mathematica version 12 (Wolfram Research, Champaign-Illinois). The goodness of fit was determined by the root mean square error method.

2.2.2 Zeta Potential Measurements

The theoretical zeta potential values were contrasted with experimentally measured zeta potential on three Al-Fh samples: an undoped Fh (0Al-Fh), 12 mol% Al substituted Fh (12Al-Fh), and 24% Al substituted Fh (24Al-Fh). Samples were precipitated from the hydrolysis of $Fe(NO_3)_3$ and $Al(NO_3)_3$ by KOH according to a modified Schwertmann and Cornell protocol (Schwertmann and Cornell 2000). Zeta potential measurements (Zetasizer Nano, Malvern Panalytical, UK) were performed in a suspension of 0.05 M $NaNO_3$, a 1:1 electrolyte, while 0.1 M NaOH was used for pH adjustments as required. The procedure for zeta potential measurements and sample synthesis has been detailed in a previous publication (Namayandeh and Kabengi 2019).

2.3 Results and Discussion

2.3.1 Placement of Al in the model

In earlier work, Manceau and Gates (2013) suggested that the Michel model (Michel et al. 2007) for Fh was incapable of explaining the experimentally derived upper limit of Al substitution into Fh. The authors used the core of the Michel model and arrived at the conclusion that Al would only substitute up to 20% of Fe. Owing to the defects present in the Michel model and the strains associated with the Fe2 and Fe3 octahedra, it is expected that these octahedra are depleted, and resulting nanoparticles of varying sizes are formed. The surface depletion model of Hiemstra (2013) and the more recent work of Boily and Song (2020) support the existence of this nanoparticle, instead of only nanocrystals with a structure akin to the Fh core of the Michel model. Replacing all of these FeOH baring Fe1 sites gives a similar value to the proposed upper limit of

24% to 29% Al substitution. During the hydrolysis of the Fe and Al ions, it is expected that Fe oligomers pre-aggregate before Al ions adsorb to the surface. Further aggregation of these nanoclusters into a nanoparticle – as the mechanism of formation is understood to be (Navrotsky 2004), would result in an Fe nanoparticle with Al sites on the exterior. According to Pinney and Morgan (2013), substitution of Al on the surface is more thermodynamically favorable than substitution in the bulk as determined via ab initio simulations. In fact, the energetics of Al-Al interactions at the surface, particularly at dilute Al concentrations are smaller compared to the energetics associated with Al substitution. Therefore, Al does not show a specific predilection towards Al segregation and clustering because of Al-Al avoidance. That is to say, as Al approaches the upper limit of substitution, it destabilizes the Fh bulk structure, and this causes Al segregation rather than Al-Al avoidance. Our interpretation of the resulting Fh nanoparticle, at various levels of Al substitution, can be observed in Figure 2.1.

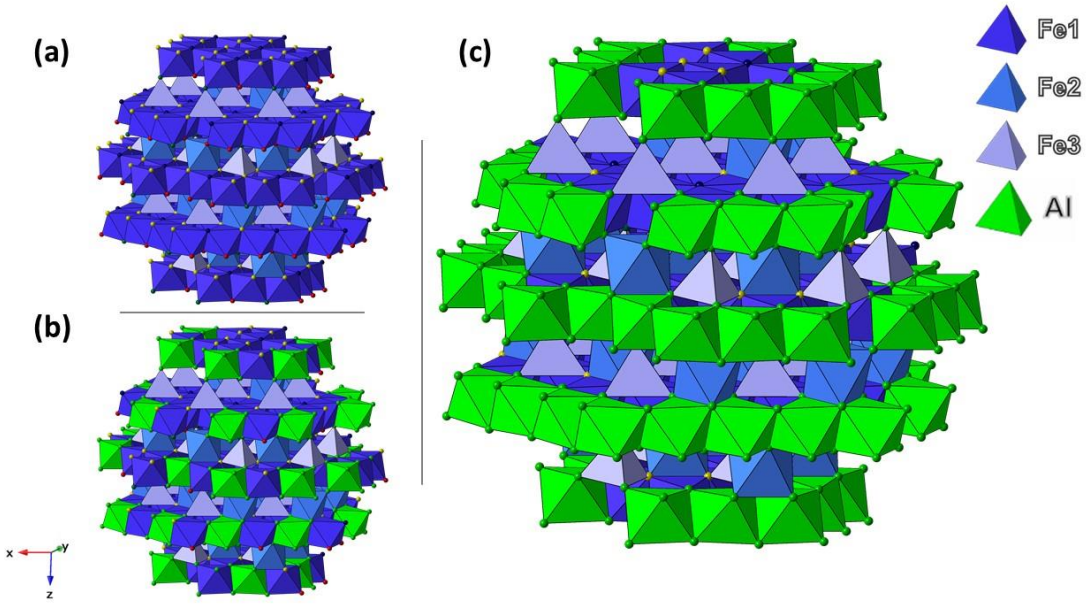

Figure 2.1. Models of Fh nanoparticles at 0 (a), 12 (b) and 24(C) mole % Al substitution representing the three samples used. In (b), Al sites (green) substitute for 12% of Fe sites equivalent to ~42% of all singly-coordinated surface groups. Similarly, for (c), 24% of Fe sites corresponding to ~84% of all singly-coordinated surface groups are replaced.

In Figure 2.1. Al (shown in green) is shown substituting for the FeOH bearing Fe1 octahedra at 12 and 24% of surface/Fe coverage. The nanoparticles derived are based on the Hiemstra surface depletion (SD) model for Fh. We want to extend our gratitude to Tjisse Hiemstra for providing us with the CrystalMaker files for the Fh model. At lower concentrations, Al is expected first to be distributed more randomly on the surface of the nanoparticle and would, where possible, avoid being seated in adjacent sites (Ducher et al. 2016) to reduce the distortion caused by the difference in metal ionic sizes. At higher Al concentrations approaching the proposed upper limit of substitution, however, Al should replace the protruding Fe1 sites resulting in alternating rings of Al octahedra, as shown in panel (c) of Figure 2.1. Research into chain monomers consisting of Al and Si (Tossell 1993) discovered that although alternating Si-Al-Si-Al linking seemed more energetically favorable, Al-Al adjacent sites could occur at higher temperatures and in disordered materials – like Fh. Chains of Al-octahedra with edge-and corner-sharing have been observed to exist (Loiseau et al. 2005), and the Al_2F_8•$2NC_5H_6$•$C_6H_3(CO_2H)_3$ synthesized in that study, spanned the *a*-axis, not unlike our proposed structure. Similarly, Al substitution in other Fe oxyhydroxides like α-FeOOH (Silva et al. 2010, Wang et al. 2014) and γ-FeOOH (Liao et al. 2020) as well as in Fh samples (Namayandeh and Kabengi 2019) has been reported to result in an increase in oxyanion adsorption as well as a reduction in the reversibility of complexes formed. These results have been attributed to an increase in inner-sphere complexation (Silva et al. 2010, Namayandeh and Kabengi 2019). In the case of Fh, the corner and edge-sharing sites having been suggested to dictate mono and bidentate bonding (Hiemstra 2013). We reason that this further proves the positioning of Al. The reader should note that we are only suggesting a structure for the Al-Fh surface, based on our interpretation of a limited set of experimental data.

In the unlikely event that doubly and triply coordinated Al sites exist on our Fh surface, these sites would probably not affect the parameterization of the electrostatic properties and hence zeta potential fitting of our SCM. This assumption is because a) the Fe2 and Fe3 sites are "recessed" within the Hiemstra structure and are not readily available for surface reactions, and b) doubly- and triply- coordinated Al sites are not pH reactive over the range under study (pH 4 - 10), and for most environmentally relevant ranges (Hiemstra et al. 1999).

2.3.2 Parameterizing the Al-surface in SCM

All sites, as expressed in Table 2.2, have sub-designations – *a* to *d* for FeOH sites, *a* to *g* for Fe_3O sites, and *a* to *d* for AlOH sites. These sub-designations were used to differentiate between sites of similar coordination, but differing in site density, face position, and affinity constants. The sites designated *s6*, *s7*, *s12*, and *s13* show the locations of Al substitution, and the boldened sections show the change in site densities of both singly-coordinated Fe and Al groups as more Al sites are included. Naturally, the undoped Fh has no sites catering to the presence of Al. It is worth mentioning that the face distribution of Al here is solely due to the replacement of singly-coordinated Fe1 sites while maintaining site density and was not arbitrarily assigned.

Table 2.2. The new properties of the undoped and Al-doped Fh surface, modified from the surface characteristics table of Hiemstra (2013). Four sites have been added, and as such, the site designations here differ from the designations used by (Hiemstra 2013).

Designation	Face	Face Distribution (%)	Type	Ns (nm^{-2})		
				0% Al-Fh	12% Al-Fh	24% Al-Fh
s1	(1-10)	37.5	FeOH*a*	1.90	**1.10**	**0.30**
s2			FeOH*b*	7.40	**4.29**	**1.18**
s3			Fe_3O*a*	3.70		
s4			Fe_3O*b*	1.90		
s5			Fe_3O*c*	3.70		
s6			**AlOH*a***	**-**	**0.80**	**1.60**
s7			**AlOH*b***	**-**	**3.11**	**6.22**
s8	(1-11)	37.5	FeOH*c*	1.60	**0.93**	**0.26**
s9			FeOH*d*	6.50	**3.77**	**1.04**
s10			Fe_3O*d*	3.30		
s11			Fe_3O*e*	3.30		
s12			**AlOH*c***	**-**	**0.67**	**1.34**
s13			**AlOH*d***	**-**	**2.73**	**5.46**
s14	(001)	12.5	Fe_3O*f*	1.10		
s15	(00-1)	12.5	Fe_3O*g*	1.10		

The physical changes introduced by the Al substitution described above impact, as expected, the chemical properties of some surface sites. For the triply coordinated sites found on the (001) and (00-1) faces, there is no substitution, and all surface parameters remain the same as for undoped Fh. The affinity constants, as expressed in **Error! Reference source not found.**, and o btained from the work of Hiemstra (2013), remain unchanged for the Fe_3O sites on these faces.

In all, there are a total of 45 complexation reactions, both protonation and electrolyte binding, accounted for in our SCM. Each of the sites involved in these reactions differs in site densities (Table 2.2). While some sites differ in charge and affinity constant values, others share those same values (Table 2.3). To reduce redundancy, only one instance of each is shown in Table

2.3. The charge and log k values for FeOH*a* and FeOH*b* are equivalent to those for FeOH*c* and FeOH*d,* respectively. Similarly, the values for FeOH*a* and FeOH*b* are equivalent to those for FeOH*c* and FeOH*d,* respectively. Fe_3O *a* to *c* groups likewise equal Fe_3O *d* to *e* groups respectively in charge and log k values while Fe_3O*g* sites are unique and do not share these parameters with other sites. Al groups replacing the Fe sites possess a protonation log k value higher than the original for that site, for example, 11 > 10.4 for AlOH*a* and FeOH*a,* respectively. The higher log k value is based on past experimental and model results for charging on Al-oxides (Hiemstra et al. 1999).

Table 2.3. Protonation and Electrolyte Complexation Reactions, Stoichiometry, Site Charge, and Equilibrium Constants.

Surface protonation			Charge	log *k*
$\equiv FeOHa^{0.5-} + H^+$	→	$\equiv FeOH_2^{0.5+}$	-0.5	10.4
$\equiv FeOHb^{0.5-} + H^+$	→	$\equiv FeOH_2^{0.5+}$	-0.5	8
$\equiv Fe_3Oa^{0.5-} + H^+$	→	$\equiv Fe_3OH^{0.5+}$	-0.5	10.4
$\equiv Fe_3Ob^{0.5-} + H^+$	→	$\equiv Fe_3OH^{0.5+}$	-0.5	5.5
$\equiv Fe_3Oc^{0.25-} + H^+$	→	$\equiv Fe_3OH^{0.75+}$	-0.25	3.3
$\equiv Fe_3Og^{0.5-} + H^+$	→	$\equiv Fe_3OH^{0.5+}$	-0.5	7.5
$\equiv AlOHa^{-0.5} + H^+$	→	$\equiv AlOH_2^{+0.5}$	-0.5	11
$\equiv AlOHb^{-0.5} + H^+$	→	$\equiv AlOH_2^{+0.5}$	-0.5	9
Electrolyte-surface interactions			**Charge**	**log *k***
$\equiv FeOH^{0.5-} + Na^+$	→	$[\equiv FeOH - Na]^{0.5+}$	-0.5	-1*
$\equiv FeOH^{0.5-} + H^+ + NO_3^-$	→	$[\equiv FeOH_2 - NO_3^-]^{-0.5}$	-0.5	-0.7*

* *Electrolyte binding constants for Na^+ and NO_3^- were held constant for all surface groups, as per the example given for FeOH. All site charges were the same as for protonation reactions.*

As shown in Table 2.3, Al sites have higher protonation pKa values than their Fe counterparts. As the contribution of these Al sites was increased in tune with our model, from 12 to 24 mole %, we observed a shift in the pH_{IEP} value to higher pH, reminiscent of Al-oxides (Figure 2.2).

Visually, model values comported with the experimental data, and the goodness of fit was determined using a weighted root mean square error (WRMSE) method. The WRNSE values obtained are 0.00217486 for 0Al-Fh, 0.00224942 for 12Al-Fh, and 0.00185706 for 24Al-Fh. Additionally, the calculated zeta potential values are within the standard error of the experimental values, as shown by the error bars in Figure 2.2.

2.3.3 Fit of model to ZP and relation to charge

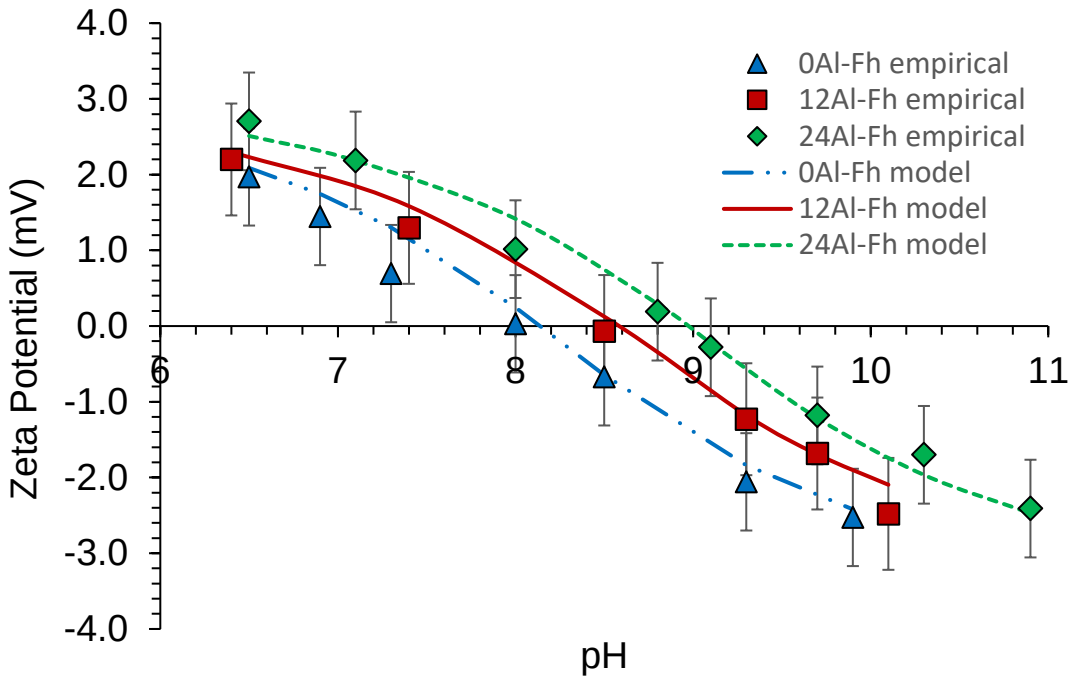

Figure 2.2. A plot of experimentally measured zeta potential values (symbols) and model-derived values (lines) for the three Al-Fh samples.

Experimental investigations and empirical modeling have suggested that the slipping plane distance, where the zeta potential is expressed, is a function of the ionic strength of the background electrolyte (Hiemstra et al. 1999, Hunter et al. 2013). Since all zeta potential measurements for our samples were carried out in suspensions of equal ionic strength, the derived slipping plane distance was similar in value - 1nm for 0Al-Fh, 1.064nm for 12Al-Fh and 1.069nm for 24Al-Fh. The points corresponding to our values were plotted on a graphical relation between ionic strength and slipping plane distance by Hiemstra et al. (1999) (Figure 2.3). Our points overlap and are in good agreement with the relation, lending weight to the fidelity of our model in simulating the zeta potential.

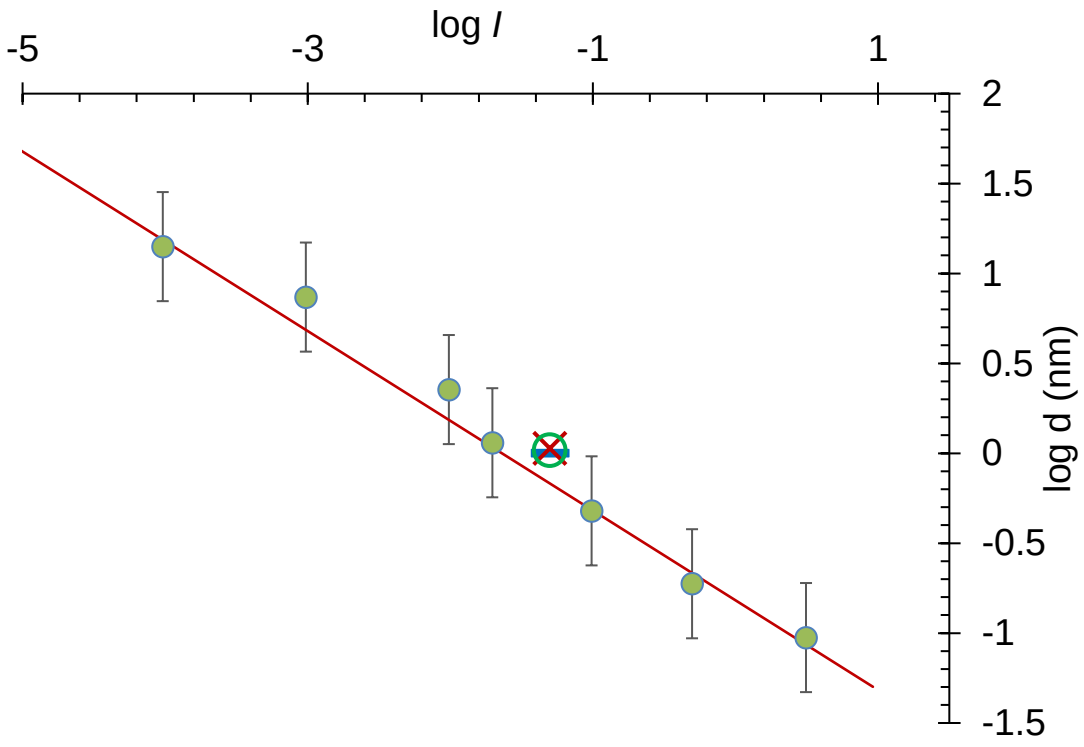

Figure 2.3. Relationship between ionic strength and the slipping plane distance. Modified from (Hiemstra et al. 1999).

2.4 Significance and Conclusion

In this work, we explore a novel SCM approach for factoring in the presence of impurities and defects on the surface of metal oxides. For Al-Fh, we hypothesize that Al substitutes for the Fe1 sites of the Fh nanoparticle and support our hypothesis with computational and spectroscopic findings from the literature. The resulting singly-coordinated Al surface sites are shown to affect surface charging and possibly, surface complexation. Our model also includes a mechanism to simulate the zeta potential of the Al-Fh surface and is successfully used to fit experimental zeta potential data. The observed shift in the pH_{IEP} for both experimental and SCM results match the trend expected for Al (hydr)oxides and further corroborate our placement of Al on the surface. The slipping plane distance obtained via SCM was consistent with previous studies, although a different metal oxide was involved, further proof that distance to be a function of the solution than the solid. This model approach is a vital step, we believe, towards the development of more accurate contaminant fate and transport models at larger scales. On the other hand, the approach discussed here can be used to provide a more realistic atom-scale representation of surfaces as used in computational models.

REFERENCES

Adra, A., G. Morin, G. Ona-Nguema & J. Brest (2016) Arsenate and arsenite adsorption onto Al-containing ferrihydrites. Implications for arsenic immobilization after neutralization of acid mine drainage. *Applied Geochemistry,* 64**,** 2-9.

Adra, A., G. Morin, G. Ona-Nguema, N. Menguy, F. Maillot, C. Casiot, O. Bruneel, S. Lebrun, F. Juillot & J. Brest (2013) Arsenic Scavenging by Aluminum-Substituted Ferrihydrites in a Circumneutral pH River Impacted by Acid Mine Drainage. *Environmental Science & Technology,* 47**,** 12784-12792.

Ainsworth, C. C., D. C. Girvin, J. M. Zachara & S. C. Smith (1989) Chromate Adsorption on Goethite: Effects of Aluminum Substitution. *Soil Science Society of America Journal,* 53**,** 411-418.

Bazilevskaya, E., D. D. Archibald, M. Aryanpour, J. D. Kubicki & C. E. Martínez (2011) Aluminum coprecipitates with Fe (hydr)oxides: Does isomorphous substitution of Al3+ for Fe3+ in goethite occur? *Geochimica et Cosmochimica Acta,* 75**,** 4667-4683.

Boily, J.-F. & X. Song (2020) Direct identification of reaction sites on ferrihydrite. *Communications Chemistry,* 3**,** 79.

Bompoti, N., M. Chrysochoou & M. Machesky (2017) Surface structure of ferrihydrite: Insights from modeling surface charge. *Chemical Geology,* 464**,** 34-45.

Carlson, L. & U. Schwertmann (1981) Natural ferrihydrites in surface deposits from Finland and their association with silica. *Geochimica et Cosmochimica Acta,* 45**,** 421-429.

Cismasu, A. C., C. Levard, F. M. Michel & G. E. Brown (2013) Properties of impurity-bearing ferrihydrite II: Insights into the surface structure and composition of pure, Al- and Si-bearing ferrihydrite from Zn(II) sorption experiments and Zn K-edge X-ray absorption spectroscopy. *Geochimica et Cosmochimica Acta,* 119**,** 46-60.

Cismasu, A. C., F. M. Michel, J. F. Stebbins, C. Levard & G. E. Brown (2012) Properties of impurity-bearing ferrihydrite I. Effects of Al content and precipitation rate on the structure of 2-line ferrihydrite. *Geochimica et Cosmochimica Acta,* 92**,** 275-291.

Corral Valero, M., B. Prelot & G. Lefevre (2019) MUSIC Speciation of gamma-Al2O3 at the Solid Liquid Interface: How DFT Calculations Can Help with Amorphous and Poorly Crystalline Materials. *Langmuir,* 35**,** 12986-12992.

Davis, J. A. & J. O. Leckie (1980) Surface ionization and complexation at the oxide/water interface. 3. Adsorption of anions. *Journal of Colloid and Interface Science,* 74**,** 32-43.

Drits, V. A., B. A. Sakharov, A. L. Salyn & A. Manceau (1993) Structural Model for Ferrihydrite. *Clay Minerals,* 28**,** 185-207.

Ducher, M., M. Blanchard, D. Vantelon, R. Nemausat & D. Cabaret (2016) Probing the local environment of substitutional Al^{3+} in goethite using X-ray absorption spectroscopy and first-principles calculations. *Physics and Chemistry of Minerals,* 43**,** 217-227.

Dzombak, D. A. & F. M. Morel. 1990. *Surface complexation modeling: hydrous ferric oxide*. John Wiley & Sons.

Fedkin, M. V., X. Y. Zhou, J. D. Kubicki, A. V. Bandura, S. N. Lvov, M. L. Machesky & D. J. Wesolowski (2003) High Temperature Microelectrophoresis Studies of the Rutile/Aqueous Solution Interface. *Langmuir,* 19**,** 3797-3804.

Gilbert, B., J. J. Erbs, R. L. Penn, V. Petkov, D. Spagnoli & G. A. Waychunas (2013) A disordered nanoparticle model for 6-line ferrihydrite. *American Mineralogist,* 98**,** 1465-1476.

Goldberg, S. 1992. Use of Surface Complexation Models in Soil Chemical Systems. In *Advances in Agronomy,* ed. D. L. Sparks, 233-329. Academic Press.

Hansel, C. M., D. R. Learman, C. J. Lentini & E. B. Ekstrom (2011) Effect of adsorbed and substituted Al on Fe(II)-induced mineralization pathways of ferrihydrite. *Geochimica et Cosmochimica Acta,* 75**,** 4653-4666.

Hawkins, T., N. Allen, M. L. Machesky, D. J. Wesolowski & N. Kabengi (2017) Ion Exchange Thermodynamics at the Rutile–Water Interface: Flow Microcalorimetric Measurements and Surface Complexation Modeling of Na–K–Rb–Cl–NO3 Adsorption. *Langmuir,* 33**,** 4934-4941.

Hiemstra, T. 2010. *Surface complexation at mineral interfaces: Multisite and Charge Distribution approach*.

--- (2013) Surface and mineral structure of ferrihydrite. *Geochimica et Cosmochimica Acta,* 105**,** 316-325.

Hiemstra, T., W. H. V. Riemsdijk, A. Rossberg & K.-U. Ulrich (2009) A surface structural model for ferrihydrite II: Adsorption of uranyl and carbonate. *Geochimica et Cosmochimica Acta,* 73**,** 4437-4451.

Hiemstra, T., W. Van Riemsdijk, G. J. J. o. c. Bolt & i. science (1989) Multisite proton adsorption modeling at the solid/solution interface of (hydr) oxides: A new approach: I. Model description and evaluation of intrinsic reaction constants. 133**,** 91-104.

Hiemstra, T. & W. H. Van Riemsdijk (1996) A Surface Structural Approach to Ion Adsorption: The Charge Distribution (CD) Model. *Journal of Colloid and Interface Science,* 179**,** 488-508.

Hiemstra, T., H. Yong & W. H. Van Riemsdijk (1999) The Interfacial Charging Phenomena of Al (hydr) oxides. *Surface complexation at mineral interfaces: Multisite and Charge Distribution approach,* 15**,** 119.

Hunter, R. J., R. H. Ottewill & R. L. Rowell. 2013. *Zeta Potential in Colloid Science: Principles and Applications*. Elsevier Science.

Johnston, C. P. & M. Chrysochoou (2016) Mechanisms of chromate, selenate, and sulfate adsorption on al-substituted ferrihydrite: implications for ferrihydrite surface structure and reactivity. *Environmental science & technology,* 50**,** 3589-3596.

Liao, S., X. Wang, H. Yin, J. E. Post, Y. Yan, W. Tan, Q. Huang, F. Liu & X. Feng (2020) Effects of Al substitution on local structure and morphology of lepidocrocite and its phosphate adsorption kinetics. *Geochimica et Cosmochimica Acta,* 276**,** 109-121.

Loiseau, T., H. Muguerra, J. Marrot, G. Férey, M. Haouas & F. Taulelle (2005) A Ladderlike Chain Aluminum Fluoride ([Al2F8]2-)n with Edge-Sharing AlF6 Octahedra. *Inorganic Chemistry,* 44**,** 2920-2925.

Machesky, M. L., M. Předota, M. K. Ridley & D. J. Wesolowski (2015) Constrained Surface Complexation Modeling: Rutile in RbCl, NaCl, and NaCF3SO3 Media to 250 °C. *The Journal of Physical Chemistry C,* 119**,** 15204-15215.

Machesky, M. L., M. K. Ridley, D. Biriukov, O. Kroutil & M. Předota (2019) Oxalic Acid Adsorption on Rutile: Experiments and Surface Complexation Modeling to 150 °C. *Langmuir,* 35**,** 7631-7640.

Machesky, M. L., D. J. Wesolowski, D. A. Palmer & K. Ichiro-Hayashi (1998) Potentiometric Titrations of Rutile Suspensions to 250°C. *Journal of Colloid and Interface Science,* 200**,** 298-309.

Manceau, A. & W. P. Gates (1997) Surface structural model for ferrihydrite. *Clays and Clay Minerals,* 45**,** 448-460.

Manceau, A. & W. P. Gates (2013) Incorporation of Al in iron oxyhydroxides: implications for the structure of ferrihydrite. *Clay Minerals,* 48**,** 481-489.

Massey, M. S., J. S. Lezama-Pacheco, F. M. Michel & S. Fendorf (2014) Uranium incorporation into aluminum-substituted ferrihydrite during iron(ii)-induced transformation. *Environmental Science: Processes & Impacts,* 16**,** 2137-2144.

Mendez, J. C. & T. Hiemstra (2019) Carbonate Adsorption to Ferrihydrite: Competitive Interaction with Phosphate for Use in Soil Systems. *ACS Earth and Space Chemistry,* 3**,** 129-141.

--- (2020) Surface area of ferrihydrite consistently related to primary surface charge, ion pair formation, and specific ion adsorption. *Chemical Geology,* 532**,** 119304.

Michel, F. M., L. Ehm, S. M. Antao, P. L. Lee, P. J. Chupas, G. Liu, D. R. Strongin, M. A. A. Schoonen, B. L. Phillips & J. B. Parise (2007) The Structure of Ferrihydrite, a Nanocrystalline Material. *Science,* 316**,** 1726.

Namayandeh, A. & N. Kabengi (2019) Calorimetric study of the influence of aluminum substitution in ferrihydrite on sulfate adsorption and reversibility. *Journal of Colloid and Interface Science,* 540**,** 20-29.

Navrotsky, A. (2004) Energetic clues to pathways to biomineralization: Precursors, clusters, and nanoparticles. *Proceedings of the National Academy of Sciences of the United States of America,* 101**,** 12096.

Pagnanelli, F., L. Bornoroni, E. Moscardini & L. Toro (2006) Non-electrostatic surface complexation models for protons and lead(II) sorption onto single minerals and their mixture. *Chemosphere,* 63**,** 1063-1073.

Pate, K. & P. Safier. 2016. 12 - Chemical metrology methods for CMP quality. In *Advances in Chemical Mechanical Planarization (CMP),* ed. S. Babu, 299-325. Woodhead Publishing.

Payne, T. E., J. A. Davis, G. R. Lumpkin, R. Chisari & T. D. Waite (2004) Surface complexation model of uranyl sorption on Georgia kaolinite. *Applied Clay Science,* 26**,** 151-162.

Pinney, N. & D. Morgan (2013) Thermodynamics of Al-substitution in Fe-oxyhydroxides. *Geochimica et Cosmochimica Acta,* 120**,** 514-530.

Reich, T. J., S. Das, C. M. Koretsky, T. J. Lund & C. J. Landry (2010) Surface complexation modeling of Pb(II) adsorption on mixtures of hydrous ferric oxide, quartz and kaolinite. *Chemical Geology,* 275**,** 262-271.

Rietra, R. P. J. J., T. Hiemstra & W. H. van Riemsdijk (1999) The relationship between molecular structure and ion adsorption on variable charge minerals. *Geochimica et Cosmochimica Acta,* 63**,** 3009-3015.

Sadeghi, O., L. N. Zakharov & M. Nyman (2015) Aqueous formation and manipulation of the iron-oxo Keggin ion. *Science,* 347**,** 1359.

Sassi, M. & K. M. Rosso (2019) Roles of Hydration and Magnetism on the Structure of Ferrihydrite from First Principles. *ACS Earth and Space Chemistry,* 3**,** 70-78.

Schwertmann, U. & R. Cornell. 2000. Iron oxides in the laboratory: Preparation and Characterization (Second, completely revised and extended edition) Wiley. Vch, Weinheim-New York-Chichester-Brisbane-Singapore-Toronto.

Silva, J., J. W. V. Mello, M. Gasparon, W. A. P. Abrahão, V. S. T. Ciminelli & T. Jong (2010) The role of Al-Goethites on arsenate mobility. *Water Research,* 44**,** 5684-5692.

Spathariotis, E. & C. Kallianou (2007) Adsorption of Copper, Zinc, and Cadmium on Goethite, Aluminum-Substituted Goethite, and a System of Kaolinite–Goethite: Surface Complexation Modeling. *Communications in Soil Science and Plant Analysis,* 38**,** 611-635.

Tossell, J. A. (1993) A theoretical study of the molecular basis of the Al avoidance rule and of the spectral characteristics of Al-O-Al linkages. *American Mineralogist,* 78**,** 911-920.

Vempati, R. K. & R. H. Loeppert (1989) Influence of Structural and Adsorbed Si on the Transformation of Synthetic Ferrihydrite. *Clays and Clay Minerals,* 37**,** 273-279.

Waite, T. D., J. A. Davis, T. E. Payne, G. A. Waychunas & N. Xu (1994) Uranium(VI) adsorption to ferrihydrite: Application of a surface complexation model. *Geochimica et Cosmochimica Acta,* 58**,** 5465-5478.

Wang, H., S. Cao, F. Kang, R. Chen, H. Liu & Y. Wei (2014) Effects of Al substitution on the microstructure and adsorption performance of α-FeOOH. *Journal of Alloys and Compounds,* 606**,** 117-123.

Zhang, Z., P. Fenter, L. Cheng, N. C. Sturchio, M. J. Bedzyk, M. Předota, A. Bandura, J. D. Kubicki, S. N. Lvov, P. T. Cummings, A. A. Chialvo, M. K. Ridley, P. Bénézeth, L. Anovitz, D. A. Palmer, M. L. Machesky & D. J. Wesolowski (2004) Ion Adsorption at the Rutile−Water Interface: Linking Molecular and Macroscopic Properties. *Langmuir,* 20**,** 4954-4969.

3 RECONCILING FLOW MICROCALORIMETRY AND DENSITY FUNCTIONAL THEORY ENTHALPIES FOR THE ADSORPTION OF PHOSPHATE, CHROMATE AND OXALATE ON RUTILE

3.1 Introduction

Adsorption is a critical and complicated process that can control the fate and transport of natural and anthropogenic contaminants in aquatic and terrestrial systems (Charbeneau 1981, Sposito 1984, Dzombak and Morel 1990). Over the last few decades, deciphering the molecular complexity of adsorption reactions at mineral-water interfaces has meant the utilization of various cutting-edge theoretical, experimental and computational techniques (Lee et al. 2013, Senftle et al. 2016, Ricci et al. 2017, Dovesi et al. 2018, Mendez and Hiemstra 2019). Each method has offered unique answers and insights into an aspect of the interface from properties of the surface (Boily and Song 2020) to those of the near-surface aqueous regions (Martin-Jimenez et al. 2016, Machesky et al. 2019). For instance, Lee et al. (2020) used resonant anomalous X-ray reflectivity (RAXR) to determine that outer-sphere species may interact more strongly with a surface than inner-sphere complexes, which is not an unprecedented notion but is uncommon (Park et al. 2008). This technique and most other spectroscopic techniques are unable to explain the driving mechanisms behind the formation of surface complexes. Computational chemistry can help by providing a better understanding of the underlying thermodynamic forces driving reactions and has been successfully used alongside other techniques to describe the nature of surfaces and surface complexes. Kubicki and Ohno (2020) calculated the free energy associated with the adsorption of phosphate on goethite using DFT and obtained results that were consistent with Infrared (IR) spectroscopy and extended X-ray absorption fine structure (EXAFS) data. An earlier study had

also successfully modeled the interaction of chromate with ferrihydrite (Kubicki et al. 2018). There, the authors compared empirically-derived attenuated total reflection Fourier transformation infrared spectroscopy (ATR-FTIR) spectra and EXAFS data with DFT calculated counterparts and found them to be consistent.

Less successful have been the attempts to directly compare experimentally-measured thermodynamic parameters to those calculated by DFT calculations, although this reconciliation is a vital step. A systematic description of the mechanisms connecting thermodynamic data, both measured and predicted, with the advanced knowledge of molecular-level structures, would afford the ability to predict macroscopic behavior based on surface reactivity. A major contributing factor to this "thermodynamic incongruence" is scaling, which remains an obstacle for quantum and molecular level simulations that remain limited by current computing power. This limitation prevents the inclusion of environmentally-relevant variables, such as ionic strength and pH variance. On the other hand, experimental methods of obtaining thermodynamic parameters, such as calorimetry (Kabengi et al. 2006a, Harvey et al. 2011) or van't Hoff analysis of batch isotherms (Malati et al. 1993, Morel et al. 2012) average data over longer time scales, meaning minutes and hours, and across the entire mineral surface and aqueous interface under study. Conversely, DFT is, relatively, a spatial and temporal snapshot involving a specific site or group of surface sites, and does not account for the energetic heterogeneity introduced by defects and various surface sites (Kabengi et al., 2017). Efforts to reconcile methodologies and benchmark experiments and calculations against each other should reduce complexity where possible, and focus on discerning the source of errors and discrepancies.

Rutile (α-TiO_2) is the most common and stable polymorph of TiO_2 The rutile (110) face is its most dominant and most thermodynamically stable face (Hanaor et al. 2012). Many

computational studies of the (110) face have been undertaken (Hiemstra et al. 1996, Fedkin et al. 2003, Předota et al. 2004, Ridley et al. 2012, Bourikas et al. 2014, Machesky et al. 2015, Predota et al. 2016, Machesky et al. 2019) making it one of the most understood surfaces among metal oxides and an archetypical system of mineral-aqueous interface studies. Additionally, nanoparticles of rutile are ideal for experimental investigations as clean, polished crystals with high surface quality are widely available (Diebold 2003). The rutile bulk structure consists of a tetragonal unit cell with Ti tetrahedra and trigonal planar coordinated O, whereas the (110) surface hosts under-coordinated Ti atoms. The resulting valency leads to the development of a surface charge and allows rutile to interact with a range of cations and anions (Diebold 2003). Oxyanions, of the formula A_xO_y, such as chromate, phosphate, sulfate, arsenate, and oxalate, to name a few, are of particular interest in earth ecosystems as they encompass both natural nutrients and hazardous contaminants (Nooney et al. 1998, Hug and Bahnemann 2006, Kabengi et al. 2006a, Luengo et al. 2006, Mendive et al. 2008). Their behavior simultaneously depends on the aqueous concentration and speciation, as well as the nature, size, and nanoscale reactivity of the mineral surfaces present. Of key interest to us are phosphate, oxalate, and chromate oxyanions. Phosphate is an essential plant nutrient in soils and, conversely, a contaminant in water bodies where it can cause eutrophication (Luengo et al. 2006). Although chromate has been widely studied due to its carcinogenic nature (Cohen et al. 1993), few studies have been conducted regarding chromate adsorption on rutile, especially since TiO_2 has been suggested as a photocatalytic instrument to immobilize chromate (Yao et al. 2010). On the other hand, oxalate sorption on rutile has been widely studied (Fahmi et al. 1995, Jones 1998, Hug and Bahnemann 2006), possibly because it is secreted by roots and helps to immobilize nutrients and contaminants (Jones 1998). Nevertheless, there are varying opinions on the energetics and complexation modes associated with its sorption

on rutile. Where some observed inner-sphere complexation (Mendive et al. 2008), others suggested this adsorption to be predominantly outer-sphere (Machesky et al. 2019).

This study aims to understand the molecular level processes causing discrepancies in theoretically derived and experimentally measured thermodynamic values. We reduce complexity by benchmarking our FAMC and DFT results in real-time using the "non-complex" rutile (110) face. For FAMC, we obtain our experimental values by measuring the heats associated with the adsorption and exchange of oxalate, chromate, and phosphate on the rutile (110) face at pH 3.0 and in a $NaNO_3$ background. We also perform DFT minimizations on a periodic rutile model using VASP and calculate the thermodynamics associated with the exchange of these oxyanions with NO_3^- and CO_3^{2-}. The kinetic and enthalpic data obtained from our FAMC analysis is compared to the theoretical thermodynamic data derived from DFT. We believe that this work will be a significant milestone towards piecing together a predictive understanding capable of tackling complex and more extensive systems.

3.2 Experimental Section

3.2.1 Solid and Chemicals

All acids, bases, and salts used in the experiment were ACS reagent grade and were used as received from Fisher Scientific (Waltham, MA). Baseline solutions of $NaNO_3$ and NaCl were prepared to a concentration of 50 mM. Oxyanion solutions of 1 mM $Na_2C_2O_4$, 1 mM NaH_2PO_4, and 1mM Na_2CrO_4 were prepared in a background solution of 47 mM $NaNO_3$ to maintain a constant ionic strength. All solutions were prepared using 18.2 MΩ deionized water and were adjusted to pH 3 ± 0.02 using either 0.1 M NaOH or 0.1 M HCl as required. The concentrations of each solution, as well as the speciation of anions in the injection solutions are presented in Table 1. The speciation data provided in Table 3.1 were obtained via Visual MINTEQ ver. 3.1.

The rutile (TiO_2) used in this work was obtained from Tioxide Specialties Ltd. (Cleveland, UK). To remove impurities, the sample underwent multiple washing-centrifuge cycles using deionized water (Ridley et al. 2009). The N_2-BET specific surface area value for the rutile sample as measured by the Brunauer-Emmet-Teller N_2-BET gas adsorption isotherm method was 17.0 m^2/g (Hawkins et al. 2017).

3.2.2 Flow Microcalorimetry Experiments

The proprietary flow adsorption microcalorimeters (FAMCs) used to conduct all sorption experiments were designed and constructed in the Kabengi Laboratory at Georgia State University. The details concerning the instrumental layout and operation of the FAMCs have been outlined in previous publications (Rhue et al. 2002, Kabengi et al. 2006a, Kabengi et al. 2006b) and in the SI. The interactions of the oxyanions with the rutile surface were investigated by measuring the heats, associated with the adsorption of the ions. The surface charge of the rutile surface was also probed using Cl^- and NO_3^-.

Exchange experiments

A mass of the rutile sample (20.0 ± 0.2 mg, 30.0 ± 0.2 mg) was packed into the instrument column and flushed with 0.05 M NaCl until a steady heat signature baseline was achieved, indicating thermal equilibrium of the solution and sample surface. To perform an exchange experiment, the solution was switched to one that had the same pH, concentration, and cation, but a different anion (0.05 M $NaNO_3$).

Table 3.1. The concentrations and speciation of ions in the experiment.

	Solution	Component	Concentration (mM)	Species Formula	% Species
Baseline	$NaNO_3$	NO_3^-	50	NO_3^-	100
	NaCl	Cl^-	50	Cl^-	100
Injection	$NaNO_3$ + NaH_2PO_4	NO_3^-	47	NO_3^-	100
		PO_4^{3-}	1	$H_2PO_4^-$	88.1
				H_3PO_4	11.9
	$NaNO_3$ + $Na_2C_2O_4$	NO_3	47	NO_3^-	100
		$C_2O_4^{2-}$	1	$HC_2O_4^-$	92.7
				$C_2O_4^{2-}$	5.7
				$H_2C_2O_4$	1.6
	$NaNO_3$ + $Na_2Cr_2O_4$	NO_3^-	47	NO_3^-	100
		CrO_4^{2-}	1	$HCrO_4^-$	93.3
				$Cr_2O_7^{2-}$	6.7

The calorimetric signal associated with NO_3^- replacing Cl^- [C/N] on the rutile surface was recorded. When the signal returned to the calorimetric baseline, the input solution was switched back to the 0.05 M $NaNO_3$ solution, and a calorimetric signal was obtained, thereby completing a cycle. This cycle was repeated for 5 days to ensure that the rutile surface had equilibrated with the baseline solutions, indicated by consistency in the heat measured during exchanges. Averages were obtained and used to calculate for the heats of exchange, Q_{exch}, expressed in $mJ/mg_{substrate}$. The exchange reactions were also used to determine the reversibility of oxyanion adsorption, further described below.

Adsorption Experiments

All adsorption experiments were carried out on rutile samples that had achieved surface equilibration. After achieving a steady baseline with 0.05 M $NaNO_3$, an injection was performed by switching the input solution to 0.047 M $NaNO_3$ + 0.001 M $Na_2C_2O_4$ for oxalate and recording

the calorimetric response generated after the signal returned to baseline. Additional exchange cycles ([C/N] and [N/C]) were performed post injection with replicates repeated until no further change in calorimetric response for Q_{exch} was recorded. The same procedure was carried out with $NaNO_3$ + NaH_2PO_4 for phosphate and $NaNO_3$ + Na_2CrO_4 for chromate. Throughout the injection experiments and during the post-injection exchange cycles, the effluent was collected, and samples were analyzed to determine the concentration of oxyanions in solution. Mass analysis for oxalate was performed at Georgia State University in Kabengi Lab using High-Performance Liquid Chromatography – Ion Conductivity (Metrohm, 881 compact IC pro) to determine the mass recovered. For phosphate, samples were digested using EPA method 30502B, and the oxyanion mass was determined by Inductively Coupled Plasma - Atomic Emission Spectroscopy (ICP-AES) using an ARL 3560 ICP analyzer at Waters Agricultural Laboratories, Inc., GA. For chromate, a Genesys 10S UV-VIS Spectrophotometer (Thermo Fisher Scientific) in Kabengi Lab at Georgia State University was used with EPA 7196A method. Mass balance calculations were then used to determine the mass adsorbed/retained and the mass desorbed for each column.

3.2.3 Density Functional Theory Calculations.

Model Details

For our work, models of the mineral-surface interactions were built and visualized using Materials Studio (BIOVIA – San Diego, CA). The (110) surface of rutile (α-TiO_2) was cleaved using the "Cleave Surface" tool from the Surface Builder in Materials Studio. Ti atoms terminating at the surface formed by the cleavage had their charges neutralized by bonding with H_2O molecules resulting in 5-coordinated Ti. The only exception to the H_2O satisfied Ti atoms was by O atoms of the adsorbate (NO_3^- or HCO_3^-) manually bonded to the surface as a bidentate bridging complex (Figure 3.1). The bidentate bridging HCO_3^- complex has been suggested to be the most likely

configuration of carbonate at the surface(Kubicki et al. 2007). A 20 Å (2 nm) vacuum space was added to the periodic surface and filled with the aqueous oxyanion compound as well as H_2O molecules to a density of 1 g/cm^3. For the carbonate exchange, the stoichiometry obtained as a result was $Ti_{80}\ O_{263}\ H_{197}\ C_1\ P_1$ for phosphate, $Ti_{80}\ O_{263}\ H_{196}\ C_1\ Cr_1$ for chromate and $Ti_{80}\ O_{263}\ H_{195}\ C_3\ Na_1$ for oxalate. The stoichiometry for oxalate replacing nitrate is given as $Ti_{80}\ O_{263}\ H_{194}\ C_2\ Na_1\ N_1$.

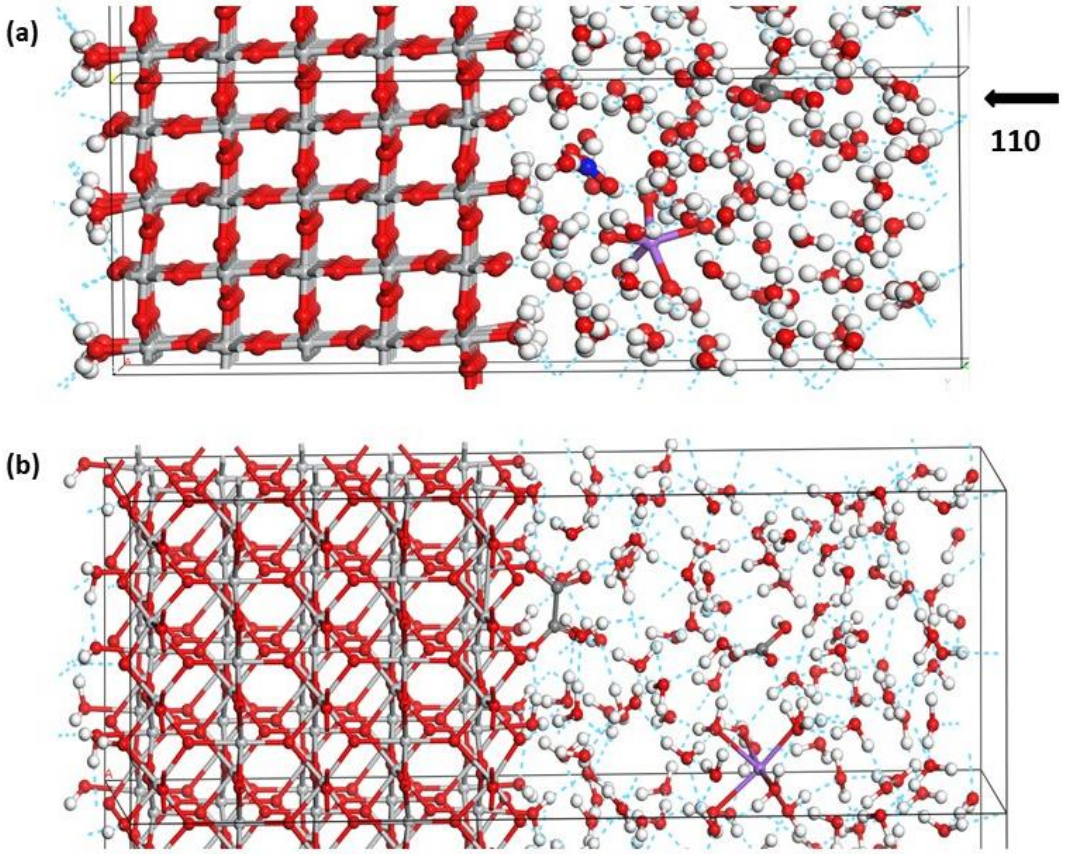

Figure 3.1. Models showing the periodic rutile (110) face with (a) Na, NO_3, and C_2O_4 in an aqueous environment and (b) HCO_3 and Na in solution while $C_2O_4^{2-}$ forms a bidentate binuclear bond with the surface.

Computational Details

While the atoms of the rutile, nitrate, and oxyanion were fixed, the H_2O molecules were relaxed with energy minimization (structural optimization) and 100 ps classical MD simulation at 300K, utilizing the Universal Force Field. Periodic calculations were performed by converting initial structures into a Vienna Ab-Initio Simulation Package (VASP Software GmbH, Austria) input format and performing energy minimizations using the PBE exchange correlation functional, a 500 eV energy cut-off and a self-interaction correction Coulomb potential, *U*, of 3 eV on Ti (Park et al. 2010). The Grimme D3 dispersion correction (Grimme et al. 2010) and fixed lattice parameters were utilized.

3.3 Results and Discussion

3.3.1 Adsorption energetics from microcalorimetry

All calorimetric responses associated with phosphate, chromate, and oxalate adsorption on rutile were positive, corresponding to an exothermic reaction. Similar responses have been measured in previous works, although the magnitudes of heats released in this work were much smaller. This smaller response peak results in a larger signal-to-noise ratio, as can be observed in Figure 3.2. Calorimetric signals associated with the adsorption of chromate, oxalate, and phosphate. An increase in voltage corresponds to the release of heat and hence, an exothermic reaction. The concentrations of each oxyanion in solution is 0.001 M. The mass of all samples in this figure is 20 ± 0.2mg.Additionally, the reactions of these oxyanions with the surface took different time to achieve calorimetric equilibrium. Even when differences in flow rates were taken into consideration, the reaction of oxalate was the fastest to return to baseline, followed by that of phosphate and finally chromate. The noted times of reactions and corresponding flow rates were

25 min and 0.283 ml/min for oxalate, 26 min and 0.323 ml/min for phosphate, and 32.3 min and 0.313 ml/min for chromate. These kinetic differences were observed on both runs of the experiments. Kinetic differences underlying sorption mechanism, namely for oxyanions, have been reported before. For instance, Laudadio et al. (2019), using FAMC, observed a two-step process in the adsorption of phosphate onto $LiCoO_2$, with an initial rapid release of heat over ~20 min followed by a slower release over ~40-60 min. This two-step process was corroborated by time-sequence in situ ATR−FTIR with two-dimensional correlation analysis that indicated that phosphate surface complexes undergo a secondary loss of water before transforming to an inner sphere bidentate mode. A similar report of a fast reaction followed by another slower step was made by Nooney et al. (1998) in their study of phosphate adsorption on TiO_2 using a similar liquid cell reaction approach, although over longer time scales of hours. Adsorption of Cr (VI) species on anatase was observed to be a slow process, and the saturation of reactive sites was suggested to have occurred after more than 24 hours (Vasileva et al. 1994).

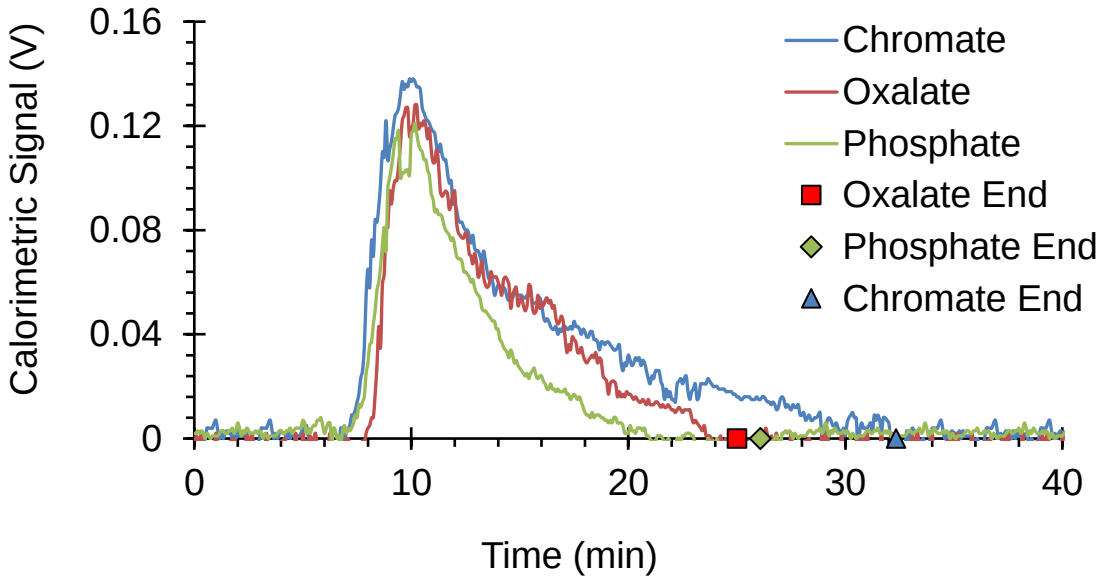

Figure 3.2. Calorimetric signals associated with the adsorption of chromate, oxalate, and phosphate. An increase in voltage corresponds to the release of heat and hence, an exothermic reaction. The concentrations of each oxyanion in solution is 0.001 M. The mass of all samples in this figure is 20 ± 0.2mg.

The heats of adsorption, Q_{ads}, for all reactions are summarized in Table 3.2. The heat released as the anions interact with the mineral surface was consistent across two runs of injections, and the measured values were averaged at –0.33 ± 0.014 mJ/mg for phosphate, –0.34 ± 0.064 mJ/mg for oxalate and –0.64 ± 0.023 mJ/mg for chromate.

Table 3.2. Summary of the heats of exchange values, enthalpies, and masses associated with the adsorption of phosphate, oxalate, and chromate onto rutile.

Specie	**Heat[1] (mJ/mg)**	**Mass adsorbed (μmol/m^2)[3]**			**Molar Enthalpy (kJ/mol)**		
		Run 1	**Run 2**	**Average**	**Run 1**	**Run 2**	**Average**
PO_4	-0.33 (0.014)[2]	-8.02E-06	-2.55E-06	-5.29E-06 (2.73E-06)[2]	-2.32	-7.94	-5.13 (3)[2]
C_2O_4	-0.34 (0.064)	-5.71E-06	-5.10E-06	-5.40E-06 (3.04E-07)	-3.40	-4.67	-4.03 (1)
CrO_4	-0.64 (0.023)	-1.32E-05	-4.95E-06	-9.08E-06 (4.13E-06)	-2.74	-7.84	-5.29 (3)

[1] *Heat values are averaged across both runs.*
[2] *Number in parentheses corresponds to the standard error of both runs.*
[3] *Surface excess calculated with a SSA value of 17.0 m^2/g*

The full mass adsorbed for each oxyanion, normalized to both sample weight and available specific surface areas, is also included in the Appendix. Two noteworthy observations can be made. First, although at the same initial concentration, the mass adsorbed for chromate in the first run was significantly higher than that calculated for phosphate and oxalate. Second, for the second experimental replicate, while the masses were more consistent with each other, the values were ~40% to ~68% lower than measured previously. Although it is imperative to obtain further replicates, the observation underscores at least qualitatively, the difficulty in accurately determining the mass adsorbed, particularly in the case of rutile that possesses a relatively low specific surface area (17.0 m^2/g in this scenario). These uncertainties are exacerbated by the fact that, at least in the case of oxalate and chromate, the complexation at the surface is expected to include a significant pool of outer-sphere species that are reversible (Yao et al. 2010, Kabengi et al. 2017, Machesky et al. 2019). It would not be possible to delineate between the heats released

from the first layer of adsorption and those form subsequent adsorption and desorption reactions of incoming ions in the flow. This obstacle is demonstrated further by the observed incongruence between the breakthrough curves and thermograms, which often trails on until calorimetric equilibrium.

The variability in determining the mass adsorbed causes a corresponding variability in the calculated molar enthalpy values, ΔH_{ads} in kJ/mol. The magnitudes of ΔH_{ads} were found to decrease in the order of $\Delta H_{ads}\ C_2O_4 > \Delta H_{ads}\ CrO_4 > \Delta H_{ads}\ PO_4$ for Run 1 and $\Delta H_{ads}\ PO_4 > \Delta H_{ads}\ CrO_4 > \Delta H_{ads}\ C_2O_4$ for Run 2. Conversely, the Q_{ads} released, independent of the surface excesses, proved more consistent for chromate and oxalate resulting in Q_{ads} chromate > Q_{ads} phosphate. Although the Q_{ads} for oxalate seems to place it in between Q_{ads} chromate and Q_{ads} phosphate in terms of magnitude, the heats for both runs of oxalate were less consistent, and could not be accurately compared to the more consistent Q_{ads} chromate and Q_{ads} phosphate values.

Juxtaposing our data with the results of other investigations proved difficult because the energetics and enthalpies of oxyanion adsorption on rutile have been largely not measured. The pH_{pzc} charge of rutile has been previously measured at 5.4 ± 0.2 (Machesky et al. 1998, Ridley et al. 2002), suggesting that under normal environmental conditions, the rutile surface is positively charged and therefore exchange and adsorption of anionic species are expected to be minimal, if not environmentally irrelevant. Nevertheless, previous work on Fe and Al (oxyhydr)oxides provide valuable insights into the nature of these oxyanions as surface complexes. For instance, Kabengi et al. (2017) report chromate adsorption to be exothermic and in inner-sphere complexation on ferrihydrite and goethite. A follow-up study by Kubicki et al. (2018), offered a nuanced reality by suggesting an equilibrium between inner-sphere and outer-sphere species distribution that depends on a number of parameters, chief among them are pH and ionic strength.

In fact, Spanos et al. (1995) observed an increase in the sorption of Cr (VI) species as pH decreased from 8.0 to 4.8 on the TiO_2 surface. However, a further reduction in pH below 4.8 resulted in less adsorption of the Cr(VI) species, implying speciation plays a vital role in ion uptake by the surface. The correlation of pH with both complexation type and speciation suggests that different species contributions to the total energetics of adsorption are likely, and an accurate account of both will be needed to rationalize the calorimetric heats, and eventually relate them to calculated values.

The difficulty in obtaining an accurate mass-balancing further highlights the role of the complexation mechanism at play. We hypothesize that for species that exhibit a more substantial portion of outer-sphere, potentially reversible species, doubts regarding the nature of the equilibrium between the flowing solution and the surface, particularly as surface coverage changes, will introduce errors in the quantification of adsorbed masses. This is specifically the case when the total mass expected to adsorbed is low (Table 3.2) owing to the lower surface areas and the inherent analytical challenge of measuring a small difference from a solution concentration under flow. A workaround would be to inject a known mass smaller than that required to achieve maximum surface coverage and thus will not break through into the effluent. An important caveat to would be to ensure detectable heats are obtained. Additional thought would also be warranted to the interpretation and values of this thermodynamic parameter far off from equilibrium.

3.3.2 DFT analysis.

Table 3.3 contains relative energies of the oxyanion-rutile (110) models simulated with 3-D periodic DFT calculations. The modeled adsorption energies calculated for phosphate and chromate exchange are both exothermic, while that of either nitrate or carbonate for oxalate is endothermic. The net ΔE_{ads} values for oxalate replacing nitrate is less favorable than that for

oxalate replacing carbonate. This result highlights the important role of the background chemistries, namely, as these ΔE_{ads} are compared to measured ΔH_{ads} where CO_2 is not completely stripped. For phosphate and chromate where the experiment and the calculation concur on the enthalpic sign, it is worth noting that the ΔE_{ads} values are significantly more negative than the ΔH_{ads}. In all, the trend of ΔE_{ads} obtained via DFT does not concur with the observed order of ΔH_{ads}.

Table 3.3. DFT Model adsorption energies (ΔE) for various oxyanions adsorbed to the rutile (110) surface.

Inner-sphere/Aqueous	**Energy (eV)**	**ΔE (kJ/mol)**
$CO_3^{2-}/H_2PO_4^-$	-3567.42093	
HPO_4^{2-}/H_2CO_3	-3568.0648	-62
$CO_3^{2-}/H_2CrO_4^-$	-3562.34801	
$HCrO_4^{2-}/H_2CO_3$	-3562.75207	-39
$CO_3^{2-}/C_2O_4^-$	-3569.91585	
$C_2O_4^{2-}/HCO_3^-$	-3569.85603	+6
$NO_3^-/C_2O_4^{2-}$	-3564.54827	
$C_2O_4^{2-}/NO_3^-$	-3564.11892	+41

There are numerous reasons for the discrepancy between the ΔE_{ads} and ΔH_{ads}. As has already been reiterated, the difficulty in determining the mass retained on the rutile surface during the calorimetry experiments results in an underestimation of the ΔH. Additionally, while FAMC inherently averages the energetic over several sites and a mixture of species, DFT is calculating a case of much lower surface coverage where bidentate binuclear species are the only ones assumed to be present. The issue of speciation is multifaceted and cuts across both techniques. For example, oxalate exists across three species at pH 3of $HC_2O_4^-$, $C_2O_4^{2-}$ and $H_2C_2O_4$, although the contribution of the latter is negligible ~1.6%. However, this implies that different concentrations of various specifications are at play aside the one calculated for. In fact, only ~5.7% of oxalate occurs as $C_2O_4^{-2}$. The DFT calculations do not capture these nuances in the results, further driving the

variation. Finally, the presence of CO_2 as a competitive adsorbate is not accounted for in DFT. Although the FAMC is equipped with a CO_2 scrubber, Villalobos and Leckie (2000) have shown that even minuscule amounts of CO_2 in a system can affect surface charging and hence complexation.

In our study, DFT calculations were performed with PBE exchange-correlation functionals, which work well for metals. However, since our work involves a metal oxide – aqueous interface, we suspect an overestimation in band gap between the highest occupied molecular orbital (HOMO) and the lowest unoccupied molecular orbital (LUMO). These errors would propagate through calculations of the bonds present, and the electronic structure of both the surface and oxyanion.

3.4 Significance and conclusions

In this chapter, we investigate the adsorption of oxyanions on rutile (110) using FAMC and DFT with the goal of benchmarking the techniques against each other. For FAMC, we measure the heats associated with the adsorption of phosphate, chromate, and oxalate on rutile at pH 3.00 ± 0.2. We obtain heat trends that hint at the prowess of our calorimetric technique but are unable to obtain consistent molar enthalpies due to the minute masses adsorbed. We also run DFT calculations on a periodic rutile surface and calculate energies associated with the exchange of NO_3 and HCO_3 with the oxyanions mentioned earlier. The DFT calculated molar enthalpies had similar trends with the heats measured via FAMC but exhibited and endothermic exchange for oxalate where FAMC was exothermic. We were unable to acquire consistent molar enthalpies from FAMC analysis. Due to the low masses adsorbed on the rutile surface during our oxyanion injections, consistent ΔH was not obtained and could not be reconciled with the ΔE obtained via DFT calculations.

Among other possible reasons, we believe the speciation of ions, masses adsorbed, the presence of and competitive uptake CO_2, as well as the choice of exchange and correlation functionals, influenced the variations in our results. This work is an important stepping stone towards discerning the complexity of interfacial reactions and reveals possible avenues of improvements for future experimental and computational investigations.

Note:

The DFT calculations were performed by Prof. James D. Kubicki at the University of Texas-El Paso.

REFERENCES

Agency, U. E. P. 1992. Method 7196A: Chromium, hexavalent (colorimetric). US Environmental Protection Agency Washington, DC.

Boily, J.-F. & X. Song (2020) Direct identification of reaction sites on ferrihydrite. *Communications Chemistry,* 3**,** 79.

Bourikas, K., C. Kordulis & A. Lycourghiotis (2014) Titanium Dioxide (Anatase and Rutile): Surface Chemistry, Liquid–Solid Interface Chemistry, and Scientific Synthesis of Supported Catalysts. *Chemical Reviews,* 114**,** 9754-9823.

Charbeneau, R. J. (1981) Groundwater contaminant transport with adsorption and ion exchange chemistry: Method of characteristics for the case without dispersion. *Water Resources Research,* 17**,** 705-713.

Cohen, M. D., B. Kargacin, C. B. Klein & M. Costa (1993) Mechanisms of Chromium Carcinogenicity and Toxicity. *Critical Reviews in Toxicology,* 23**,** 255-281.

Diebold, U. (2003) The surface science of titanium dioxide. *Surface Science Reports,* 48**,** 53-229.

Dovesi, R., A. Erba, R. Orlando, C. M. Zicovich-Wilson, B. Civalleri, L. Maschio, M. Rérat, S. Casassa, J. Baima, S. Salustro & B. Kirtman (2018) Quantum-mechanical condensed matter simulations with CRYSTAL. 8**,** e1360.

Dzombak, D. A. & F. M. Morel. 1990. *Surface complexation modeling: hydrous ferric oxide*. John Wiley & Sons.

Fahmi, A., C. Minot, P. Fourré & P. Nortier (1995) A theoretical study of the adsorption of oxalic acid on TiO2. *Surface Science,* 343**,** 261-272.

Fedkin, M. V., X. Y. Zhou, J. D. Kubicki, A. V. Bandura, S. N. Lvov, M. L. Machesky & D. J. Wesolowski (2003) High Temperature Microelectrophoresis Studies of the Rutile/Aqueous Solution Interface. *Langmuir,* 19**,** 3797-3804.

Grimme, S., J. Antony, S. Ehrlich & H. Krieg (2010) A consistent and accurate ab initio parametrization of density functional dispersion correction (DFT-D) for the 94 elements H-Pu. *The Journal of Chemical Physics,* 132**,** 154104.

Hanaor, D. A. H., W. Xu, M. Ferry & C. C. Sorrell (2012) Abnormal grain growth of rutile TiO2 induced by ZrSiO4. *Journal of Crystal Growth,* 359**,** 83-91.

Harvey, O. R., B. E. Herbert, R. D. Rhue & L.-J. Kuo (2011) Metal Interactions at the Biochar-Water Interface: Energetics and Structure-Sorption Relationships Elucidated by Flow Adsorption Microcalorimetry. *Environmental Science & Technology,* 45**,** 5550-5556.

Hawkins, T., N. Allen, M. L. Machesky, D. J. Wesolowski & N. Kabengi (2017) Ion Exchange Thermodynamics at the Rutile–Water Interface: Flow Microcalorimetric Measurements and Surface Complexation Modeling of Na–K–Rb–Cl–NO3 Adsorption. *Langmuir,* 33**,** 4934-4941.

Hiemstra, T., P. Venema & W. H. V. Riemsdijk (1996) Intrinsic Proton Affinity of Reactive Surface Groups of Metal (Hydr)oxides: The Bond Valence Principle. *Journal of Colloid and Interface Science,* 184**,** 680-692.

Hug, S. J. & D. Bahnemann (2006) Infrared spectra of oxalate, malonate and succinate adsorbed on the aqueous surface of rutile, anatase and lepidocrocite measured with in situ ATR-FTIR. *Journal of Electron Spectroscopy and Related Phenomena,* 150**,** 208-219.

Jones, D. L. (1998) Organic acids in the rhizosphere – a critical review. *Plant and Soil,* 205**,** 25-44.

Kabengi, N. J., M. Chrysochoou, N. Bompoti & J. D. Kubicki (2017) An integrated flow microcalorimetry, infrared spectroscopy and density functional theory approach to the study of chromate complexation on hematite and ferrihdyrite. *Chemical Geology,* 464**,** 23-33.

Kabengi, N. J., S. H. Daroub & R. D. Rhue (2006a) Energetics of arsenate sorption on amorphous aluminum hydroxides studied using flow adsorption calorimetry. *J Colloid Interface Sci,* 297**,** 86-94.

Kabengi, N. J., R. D. Rhue & S. H. Daroub (2006b) Using Flow Calorimetry to Determine the Molar Heats of Cation and Anion Exchange and the Point of Zero Net Charge on Amorphous Aluminum Hydroxides. *Soil Science,* 171**,** 13-20.

Kubicki, J. D., N. Kabengi, M. Chrysochoou & N. Bompoti (2018) Density functional theory modeling of chromate adsorption onto ferrihydrite nanoparticles. *Geochemical transactions,* 19**,** 8.

Kubicki, J. D., K. D. Kwon, K. W. Paul & D. L. Sparks (2007) Surface complex structures modelled with quantum chemical calculations: carbonate, phosphate, sulphate, arsenate and arsenite. *European Journal of Soil Science,* 58**,** 932-944.

Kubicki, J. D. & T. Ohno (2020) Integrating Density Functional Theory Modeling with Experimental Data to Understand and Predict Sorption Reactions: Exchange of Salicylate for Phosphate on Goethite. *Soil Systems,* 4**,** 27.

Laudadio, E. D., P. Ilani-Kashkouli, C. M. Green, N. J. Kabengi & R. J. Hamers (2019) Interaction of Phosphate with Lithium Cobalt Oxide Nanoparticles: A Combined Spectroscopic and Calorimetric Study. *Langmuir,* 35**,** 16640-16649.

Lee, S. S., P. Fenter & C. Park (2013) Optimizing a flow-through X-ray transmission cell for studies of temporal and spatial variations of ion distributions at mineral-water interfaces. *Journal of Synchrotron Radiation,* 20**,** 125-136.

Lee, S. S., C. Park, N. C. Sturchio & P. Fenter (2020) Nonclassical Behavior in Competitive Ion Adsorption at a Charged Solid–Water Interface. *The Journal of Physical Chemistry Letters,* 11**,** 4029-4035.

Luengo, C., M. Brigante, J. Antelo & M. Avena (2006) Kinetics of phosphate adsorption on goethite: Comparing batch adsorption and ATR-IR measurements. *Journal of Colloid and Interface Science,* 300**,** 511-518.

Machesky, M. L., M. Předota, M. K. Ridley & D. J. Wesolowski (2015) Constrained Surface Complexation Modeling: Rutile in RbCl, NaCl, and NaCF3SO3 Media to 250 °C. *The Journal of Physical Chemistry C,* 119**,** 15204-15215.

Machesky, M. L., M. K. Ridley, D. Biriukov, O. Kroutil & M. Předota (2019) Oxalic Acid Adsorption on Rutile: Experiments and Surface Complexation Modeling to 150 °C. *Langmuir,* 35**,** 7631-7640.

Machesky, M. L., D. J. Wesolowski, D. A. Palmer & K. Ichiro-Hayashi (1998) Potentiometric Titrations of Rutile Suspensions to 250°C. *Journal of Colloid and Interface Science,* 200**,** 298-309.

Malati, M. A., R. A. Fassam & I. R. Henderson (1993) Mechanism of phosphate interaction with two reference clays and an anatase pigment. 58**,** 387-389.

Martin-Jimenez, D., E. Chacon, P. Tarazona & R. Garcia (2016) Atomically resolved three-dimensional structures of electrolyte aqueous solutions near a solid surface. *Nature Communications,* 7**,** 12164.

Mendez, J. C. & T. Hiemstra (2019) Carbonate Adsorption to Ferrihydrite: Competitive Interaction with Phosphate for Use in Soil Systems. *ACS Earth and Space Chemistry,* 3**,** 129-141.

Mendive, C. B., T. Bredow, A. Feldhoff, M. Blesa & D. Bahnemann (2008) Adsorption of oxalate on rutile particles in aqueous solutions: a spectroscopic, electron-microscopic and theoretical study. *Physical Chemistry Chemical Physics,* 10**,** 1960-1974.

Morel, J.-P., N. Marmier, C. Hurel & N. Morel-Desrosiers (2012) Effect of temperature on the sorption of europium on alumina: Microcalorimetry and batch experiments. *Journal of Colloid and Interface Science,* 376**,** 196-201.

Nooney, M. G., A. Campbell, T. S. Murrell, X. F. Lin, L. R. Hossner, C. C. Chusuei & D. W. Goodman (1998) Nucleation and Growth of Phosphate on Metal Oxide Thin Films. *Langmuir,* 14**,** 2750-2755.

Park, C., P. A. Fenter, N. C. Sturchio & K. L. Nagy (2008) Thermodynamics, Interfacial Structure, and pH Hysteresis of Rb+ and Sr2+ Adsorption at the Muscovite (001)−Solution Interface. *Langmuir,* 24**,** 13993-14004.

Park, S.-G., B. Magyari-Köpe & Y. Nishi (2010) Electronic correlation effects in reduced rutile **TiO_2** within the **LDA+*U*** method. *Physical Review B,* 82**,** 115109.

Předota, M., A. V. Bandura, P. T. Cummings, J. D. Kubicki, D. J. Wesolowski, A. A. Chialvo & M. L. Machesky (2004) Electric Double Layer at the Rutile (110) Surface. 1. Structure of Surfaces and Interfacial Water from Molecular Dynamics by Use of ab Initio Potentials. *The Journal of Physical Chemistry B,* 108**,** 12049-12060.

Predota, M., M. L. Machesky & D. J. Wesolowski (2016) Molecular Origins of the Zeta Potential. *Langmuir,* 32**,** 10189-10198.

Rhue, R., C. Appel & N. Kabengi (2002) Measuring surface chemical properties of soil using flow calorimetry 1. *Soil science,* 167**,** 782-790.

Ricci, M., W. Trewby, C. Cafolla & K. Voïtchovsky (2017) Direct observation of the dynamics of single metal ions at the interface with solids in aqueous solutions. *Scientific Reports,* 7**,** 43234.

Ridley, M. K., T. Hiemstra, M. L. Machesky, D. J. Wesolowski & W. H. van Riemsdijk (2012) Surface speciation of yttrium and neodymium sorbed on rutile: Interpretations using the charge distribution model. *Geochimica et Cosmochimica Acta,* 95**,** 227-240.

Ridley, M. K., T. Hiemstra, W. H. van Riemsdijk & M. L. Machesky (2009) Inner-sphere complexation of cations at the rutile–water interface: A concise surface structural interpretation with the CD and MUSIC model. *Geochimica et Cosmochimica Acta,* 73**,** 1841-1856.

Ridley, M. K., M. L. Machesky, D. A. Palmer & D. J. Wesolowski (2002) Potentiometric studies of the rutile–water interface: hydrogen-electrode concentration-cell versus glass-electrode titrations. *Colloids and Surfaces A: Physicochemical and Engineering Aspects,* 204**,** 295-308.

Senftle, T. P., S. Hong, M. M. Islam, S. B. Kylasa, Y. Zheng, Y. K. Shin, C. Junkermeier, R. Engel-Herbert, M. J. Janik, H. M. Aktulga, T. Verstraelen, A. Grama & A. C. T. van Duin (2016) The ReaxFF reactive force-field: development, applications and future directions. *npj Computational Materials,* 2**,** 15011.

Spanos, N., S. Slavov, C. Kordulis & A. Lycourghiotis (1995) Mechanistic aspects of the deposition of the Cr(VI) species on the surface of TiO2 and SiO2. *Colloids and Surfaces A: Physicochemical and Engineering Aspects,* 97**,** 109-117.

Sposito, G. 1984. *The surface chemistry of soils*. Oxford university press.

Vasileva, E., K. Hadjiivanov & P. Mandjukov (1994) Adsorption of Cr6+ oxo anions on pure and peroxide-modified TiO2 (anatase). *Colloids and Surfaces A: Physicochemical and Engineering Aspects,* 90**,** 9-15.

Villalobos, M. & J. O. Leckie (2000) Carbonate adsorption on goethite under closed and open CO2 conditions. *Geochimica et Cosmochimica Acta,* 64**,** 3787-3802.

Yao, Z., F. Jia, Y. Jiang, C. Li, Z. Jiang & X. Bai (2010) Photocatalytic reduction of potassium chromate by Zn-doped TiO2/Ti film catalyst. *Applied Surface Science,* 256**,** 1793-1797.

4 CONCLUSIONS

This thesis explored the different ways experiments and theory could be interlinked to describe interfacial reactions involving minerals and aqueous solutions. A consistent theme of this work is complexity. As such, the first part focuses on capturing the complexity of interfaces by developing an approach to account for surface defects/substitution in models that will be a more accurate description of "real" co-precipitated mineral oxide surfaces. The second section of this work acknowledges the complexity of interfaces and seeks to constrain it to examine the sources of errors introduced by two techniques used to derive thermodynamics parameters. One technique views the interface from the lens of solution chemistry while the other focuses on an atomistic-view of the interface.

In Chapter 2, we developed a novel SCM model that successfully modeled experimental zeta potential measurements of Al-Fh surfaces. It consists of a surface structure model for Al-Fh that we inferred by considering the implications of the upper limit of Al substitution (~ 24 mol %) as determined by spectroscopic techniques. With insights from computational modeling results that highlighted the most stable sites for replacement, we situated Al on the surface of Fh and hypothesized that it is replacing Fe1 sites. The resulting surface model for Al-Fh, based on Hiemstra's surface depletion model, has Al forming chain-like structures at the upper limit of substitution. We also inferred that the placement of these in place of edge and corner-sharing Fe sites plays a significant role in controlling inner-sphere to outer-sphere species ratio, which is commonly reported to be perturbed as an effect of Al substitution. The zeta potential model developed fit experimental measurements successfully and to a reasonable degree of certainty. These zeta potential values are the surface potential "measured" at a distance from the surface, referred to as the slipping plane distance. In our work, we measured that potential at ~10 Å (~1

nm) from the surface. Coupled with our suspension concentration of 0.05M, the results obtained were consistent with previous empirical data that showed the slipping plane distance to be a function of the ionic strength of the solution.

Chapter 3 of this work examined the enthalpies, both measured and calculated, of phosphate, chromate, and oxalate sorption on the rutile (110) crystal face. The goal was to benchmark FAMC and DFT against each other to better understand the underlying sources of errors that have made the reconciliation of computational results and experimental thermodynamics elusive. FAMC was used to measure the heats associated with the adsorption of phosphate, chromate, and oxalate in a background of 0.05M $NaNO_3$ at pH 3. Mass analysis was also performed on effluent collected during the injection run to determine the mass of oxyanions adsorbed. The heat and mass values obtained were used to calculate the molar enthalpies of adsorption. DFT calculations were performed on a periodic model of the rutile (110) face terminating at the aqueous interface with the oxyanions in solution. Energy minimizations were performed using VASP with PBE exchange correlation functionals, a 500 eV energy cut-off, a 3 eV U self-interaction correction on Ti, a D3 dispersion correction, and fixed lattice parameters. Due to the small masses adsorbed on the rutile surface during oxyanion injections, consistent ΔH_{ads} was not obtained, and could not be reconciled with the ΔE_{ads} obtained via DFT calculations. Instead, ΔE_{ads} aligned with Q_{ads}.

4.1 Future Work

Although the novel approach discussed in Chapter 2 helps us account for defects, there are aspects of Al-Fh that are still not completely understood. For example, Fh is known to possess an amorphous phase(Funnell et al. 2020), which may contribute to charging and adsorption.

Unfortunately, this phase of the mineral is not captured in any SCM modeling efforts. Additionally, Fh aggregates into nanoparticles of different sizes, and accounting for the corresponding change in site densities and possibly face contributions should provide a better fit with future models. Since we insinuate the participation of Al at specific faces to surface complexation, future works may focus on an intersection of an imaging technique like Transmission Electron Microscopy (TEM) with a powerful spectroscopic technique like RAXR that would help pinpoint the proximity of ionic species to the Al-Fh surface. These techniques, using a host of cations and anions that form inner- and outer-sphere complexes, coupled with this SCM model, should result in an accurate and concrete description of the Al-Fh surface. In a broader sense, the approach we utilized to develop this SCM opens the door to much improved ways to capture complexity and could be applied to multiphase minerals with more complex surfaces.

For Chapter 3, two thermodynamic techniques were benchmarked against each other using a “simple” surface. The heats for FAMC were replicable, but the masses adsorbed were so small that minor deviations were relatively very substantial. We could remedy this obstacle by injecting known smaller masses that would reach total surface coverage. Additionally, the pH at which experiments were carried out, pH 3, resulted in a complex speciation profile that is difficult to account for. The divergence in the DFT results may have also been a function of the exchange correlation functionals used since DFT with PBE works well for metals, and B3LYP works better for oxides. A hybrid Hartree-Fock and DFT method for the periodic model, with cluster models running in Gaussian basis sets and using B3LYP functionals, would possibly provide more accurate results. An alternative would be to carry out both FAMC experiments and DFT calculations on a non-oxide mineral surface, eliminating the need to account for oxides. A successful reconciliation of FAMC and DFT may be the gateway to break down and parameterize

molecular thermodynamic processes, leading to models that are capable of accurately predicting thermodynamic attributes, and subsiding the need for intensive experimental work.

REFERENCES

Funnell, N. P., M. F. Fulford, S. Inoué, K. Kletetschka, F. M. Michel & A. L. Goodwin (2020) Nanocomposite structure of two-line ferrihydrite powder from total scattering. *Communications Chemistry*, 3**,** 22.